NAVAL POSTGRADUATE SCHOOL
Monterey, California

DTIC
ELECTE
MAR 15 1993
S
B

THESIS

INVESTIGATION OF A BACKGROUND SUPPRESSION TRANSIMPEDANCE
AMPLIFIER FOR PHOTOVOLTAIC DETECTORS.

by

Ferdinand Joseph Metzger Jr.

December, 1992

Thesis Advisor: D.S. Davis
Second Reader: A.A. Atchley

93-05287

93 3 12 034

REPORT DOCUMENTATION PAGE

1a Report Security Classification Unclassified	1b Restrictive Markings
2a Security Classification Authority	3 Distribution Availability of Report:
2b Declassification/Downgrading Schedule	Approved for public release; distribution is unlimited.
4 Performing Organization Report Number(s)	5 Monitoring Organization Report Number(s)

6a Name of Performing Organization Naval Postgraduate School	6b Office Symbol (If Applicable) PH/Dv	7a Name of Monitoring Organization Naval Postgraduate School
6c Address (city, state, and ZIP code) Monterey, CA 93943-5000		7b Address (city, state, and ZIP code) Monterey, CA 93943-5000
8a Name of Funding/Sponsoring Organization NPS	8b Office Symbol (If Applicable)	9 Procurement Instrument Identification Number
8c Address (city, state, and ZIP code)		10 Source of Funding Numbers

10		

Program Element Number	Project No	Task No	Work Unit Accession No

11 Title (Include Security Classification) INVESTIGATION OF A BACKGROUND SUPPRESSION TRANSIMPEDANCE AMPLIFIER FOR PHOTOVOLTAIC DETECTORS.

12 Personal Author(s) Ferdinand J. Metzger Jr.

13a Type of Report Master's Thesis	13b Time Covered From To	14 Date of Report (year, month,day) December 1992	15 Page Count 70

16 Supplementary Notation The views expressed in this thesis are those of the author and do not reflect the official policy or position of the Department of Defense or the U.S. Government.

17 Cosati Codes			18 Subject Terms (continue on reverse if necessary and identify by block number)
Field	Group	Subgroup	background suppression, transimpedance amplifier, photovoltaic detector

19 Abstract (continue on reverse if necessary and identify by block number
   The current generation of transimpedance amplifier based detector systems are limited by opamp saturation when operating at a high gain or in the presence of a large background signal. To eliminate saturation, an amplifier that is frequency dependent is developed. Additionally, the noise sources in the conventional transimpedance amplifier and photovoltaic detector are quantified for comparison to any modified circuit. Initial results indicate that the frequency dependent detector system is a viable system, however, further development is required. Further research of this technology is expected to support future infrared and long range detection applications.

20 Distribution/Availability of Abstract [X] unclassified/unlimited [ ] same as report [ ] DTIC users	21 Abstract Security Classification Unclassified
22a Name of Responsible Individual D.S. Davis	22b Telephone (Include Area code) (408) 646-2877	22c Office Symbol PH/Dv

DD FORM 1473, 84 MAR   83 APR edition may be used until exhausted   security classification of this page

All other editions are obsolete   Unclassified

INVESTIGATION OF A BACKGROUND SUPPRESSION TRANSIMPEDANCE AMPLIFIER FOR PHOTOVOLTAIC DETECTORS.

by

Ferdinand Joseph Metzger Jr.

Lieutenant, United States Navy
B.S., University of the State of New York, 1985

Submitted in partial fulfillment of the
requirements for the degree of
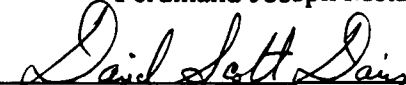
MASTER OF SCIENCE IN ENGINEERING SCIENCE

from the

NAVAL POSTGRADUATE SCHOOL

December, 1992

Author: _____
Ferdinand Joseph Metzger Jr.

Approved by: _____
D.S. Davis, Thesis Advisor

_____
A.A. Atchley, Second Reader

_____
K.E. Woehler, Chairman,
Department of Physics

ABSTRACT

The current generation of transimpedance amplifier based detector systems are limited by opamp saturation when operating at a high gain or in the presence of a large background signal. To eliminate saturation, an amplifier that is frequency dependent is developed. Additionally, the noise sources in the conventional transimpedance amplifier and photovoltaic detector are quantified for comparison to any modified circuit. Initial results indicate that the frequency dependent detector system is a viable system, however, further development is required. Further research of this technology is expected to support future infrared and long range detection applications.

iii

I. INTRODUCTION

All objects emit electromagnetic radiation, or photons, by virtue of the fact that they have a finite temperature. These photons can then be detected by a system designed to detect a photon of the given wavelength. As an example, human eyes detect incident photons that are between 4000 and 7000 Angstroms only. Photons outside this range are not sensed by the eye. The detectors of photons in an electronic system is referred to as opto-electronic detector. Opto-electronic detectors utilize the ability of a specific material to change an electrical characteristic of the detector in the presence of a photon. These detectors can be grouped into two categories with distinct characteristics.

The first category consists of detectors that respond to the average power absorbed by the detector and are not dependent on the quantum nature of the electromagnetic radiation field. The incident power changes a thermodynamic property of the detector which is then measured as an output, such as a bolometer which detects a change in temperature of the system.

The second category consists of the quantum detectors. These detectors respond as a direct consequence of the absorption of optical quanta, or photons. They are responsive to photons incident on the surface. Common examples of this type of detector are those that use the photoelectric effect. These devices include photocells, photomultipliers, and photovoltaic diodes. This is the category of detectors that will be examined in this thesis research. Specifically, the photovoltaic diode or photodiode will be used throughout this thesis research.

As the sophistication of solid-state physics increased over the last 50 years, the number of solid state detectors also expanded proportionally. The current proliferation of efficient photovoltaic quantum detectors have allowed an ever expanding list of applications

as each new generation of detectors has been introduced. The detector system developed under this thesis is an extension of this development.

A typical solid state photovoltaic detector is a simple semiconductor P-N junction. An incident photon can, provided it has sufficient energy, create an electron-hole pair. This pair can then migrate through the detector to be output as a tiny quantum of current flowing across the junction. In order to produce a signal that is linearly proportional to the created current flow at the P-N junction, a high gain current to voltage system is necessary. This system, known as a transimpedance amplifier, normally consists of a photodetector, an operational amplifier (opamp) with a high gain and input impedance, and a high resistance feedback resistor. These three components produce an output voltage that is proportional to the product of the detector photocurrent and the feedback resistance.

The most sensitive detection system uses a large feedback resistor value. Ideally, a system would be designed so that any photon sources (targets of interest) would give a signal that is substantially higher than the noise created by the systems electronics or introduced by the environment. This forces a compromise between two competing forces when choosing a feedback resistor since it is this component that determines both the sensitivity and the bulk of the noise. The resistor must be large in order to produce a usable signal, but it cannot be too large or the opamp output will be saturated. Additionally, an increase in the resistance will increase the Johnson noise which significantly deteriorates the system's performance.

The transimpedance system as described above does not work well in the mid-infrared region (2 to 20 μm). In this region the ambient thermal background photon flux is normally higher than the target signal. This large background photon flux has two undesirable effects on a detector. First, it causes the transimpedance amplifier system to saturate even when a low feedback resistance is used. Secondly, the background photons arrive randomly and at all frequencies. This creates an enormous background noise that

2

significantly limits the effectiveness of the system. These effects make the detection of a weak source in this region extremely difficult.

The object of this thesis research has been to study a way to circumvent these problems, at least to a first approximation. It is the opamp that is the weak link in the transimpedance detection system. The P-N junction photodetector does not normally saturate when the system is saturated. The P-N junction continues to respond linearly even though the opamp is saturated. Historically, is has been necessary to lower the value of the feedback resistor to compensate for this saturation problem. This degrades the sensitivity of the detector system, removes the saturation of the opamp and reestablishes a linear response for the system.(Boyd, 1983, pp.177-190)

The approach taken in this thesis research is to assume that the background problem can be addressed by replacing the feedback resistor with a more complex network that has a peak impedance at some tuned frequency f_O. This assumes that the source of interest can be modulated at a frequency f_O. The results of the new system will be used to detect a source in the presence of a large background signal whose noise statistics are governed by a Poisson distribution, such as that which would be present in an infrared system. The results will be contrasted with the standard transimpedance system.

Chapter II will describe the theory of operation of the standard transimpedance detection system and the abrupt P-N junction photodiode. Chapter III is the theory of thermal blackbody radiation and the thermal blackbody noise spectrum that the system will be designed to handle. Chapter IV describes the various noise sources in the detection process including all sources integral to the detector itself and the background. Chapter V discusses the method taken to correct the background saturation problem, the extended transimpedance amplifier. The experimental results are discussed in Chapter VI including a discussion of the basic and extended transimpedance amplifier circuits.

II. CONVENTIONAL TRANSIMPEDANCE DETECTION SYSTEMS

As discussed in Chapter I, the detection of incident light in the systems of interest is done by a quantum, or photon, detector. A quantum detector absorbs an incident photon directly into the detector material without first thermalizing its energy. This absorption causes a change in the populations of charge carriers in the detector's valence and conduction bands. The specific quantum detector used is the photovoltaic detector or photodiode. Photovoltaic detectors generate minute currents across P-N junctions as a result of this photon absorption. These currents are then amplified and processed by a transimpedance amplifier to produce an output voltage which is proportional to the junction current. This relationship makes the output voltage proportional to the incident photon flux. A perfect photovoltaic detector and transimpedance amplifier system will yield an average output voltage that is precisely proportional to the average incident photon flux.

In order to produce a usable linear voltage output from the detector it must be combined with an appropriate current-to-voltage converting amplifier. A transimpedance amplifier is used to provide the needed amplification and current-to-voltage characteristics of the detector circuit.

A. PHOTOVOLTAIC OPTOELECTRONIC DETECTORS

Photovoltaic detectors use the characteristics of semiconducting materials to produce an output current (and, indirectly a voltage) without any external electrical bias. The detector is usually an intrinsic semiconducting photodiode or an abrupt P-N junction photodiode.

1. Semiconductors

Some of the elements in column IV-A of the periodic table are referred to as intrinsic semiconductors. These are all elements which are characterized as having four

electrons in their outer or valence orbital shell. In their densest states, these elements combine with other atoms in order to share the outer valence electrons with its four closest neighbors. This creates a material with face-centered cubic cell structure that is mechanically rigid (Pierret, 1988 ,pg.110).

The pure atoms in this column are, however, not the only materials that exhibit the characteristics of being semiconducting. When compounds consisting of elements from columns III and V of the periodic table are produced, many of these also behave as a semiconductor.

2. The Electrical Properties of Semiconductors

The electrical properties of the solid semiconducting materials are determined by considering the energy level characteristics of the electrons in the lattice (for crystalline materials) or matrix (for amorphous materials). Quantum mechanics shows that the energy level structure of a solid consists of a ladder of bands, populated by electrons. The lower energy bands are normally completely filled with electrons, while the outer bands are completely empty. In general, there is a transition region which contains a lower energy band that is mostly filled (the valence band) and a slightly higher energy band that is mostly empty (the conduction band). Electrons in the valance band are constrained to stay within the band, while those in the conduction band are free to move about the lattice under the influence of electromagnetic fields. This structure is used to explain a basic electrical property, the electrical conductivity. Insulators have few or no electrons in their conduction bands. Conductors have many electrons in their conduction bands. Semiconductors are an intermediate case, with a moderate number of electrons in the conduction band.

The difference in energy between the top of the valence band and the bottom of the conduction band is called the band gap energy, E_g. The zero level of energy is, by convention, taken to be the top of the valence band. This band and band gap is graphically shown in Figure 2.1.
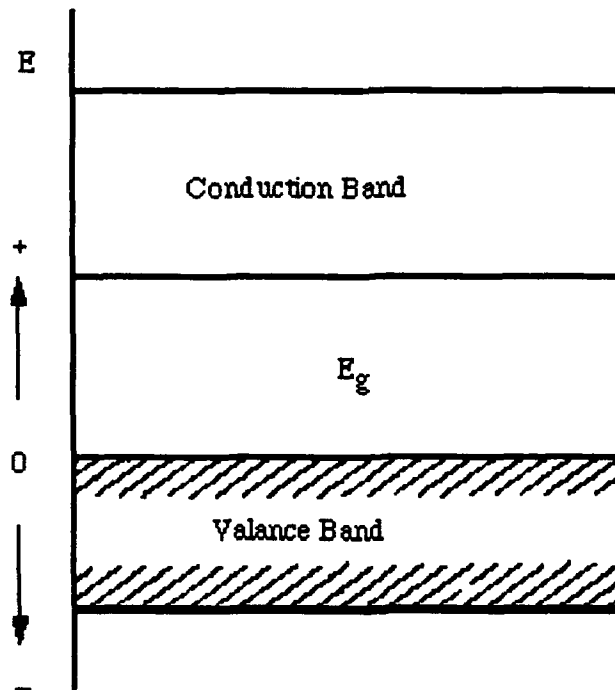
Figure 2.1 Conventional energy band gap diagram

It is this energy gap that determines the electrical characteristics of the material along with electron mobility and temperature. If the band gap is small then the energy required to cause an electron to "jump" between bands is relatively small. For this small band gap thermal agitation can provide enough energy to place large numbers of electrons in the conduction band, and the material is a conductor. A semiconductor has a band gap larger that that of a conductor, but below that of an insulator.

Any process that causes an electron to move from the valence to the conduction band leaves an unfilled region, or positive hole, in the valence band. This hole is free to move in the valence band, and provides a second mechanism for charge motion in semiconductors.

6

3. The Effects of Doping

The electrical characteristics of semiconductors are extremely sensitive to the presence of impurities. These impurities, called dopants, can dramatically change the band gap energy of the material. The impurities can create an excess of either holes or electrons. As an example, suppose a phosphorous (5 valence electrons) impurity is added to a sample of pure germanium (4 valence electrons). The crystal that is formed has germanium-like chemical bonding with 4 of the 5 phosphorous electrons, since germanium has 4 electrons in its valence shell. The fifth electron is then a "spare electron", loosely bound to the crystal. It will be free to move about the lattice, increasing the conductivity of the material. This type of material is said to be an N-type because of the excess of free electrons or negative charges. If the germanium is doped with an element with only three electrons in its valence band, then we can see by the same reasoning that there will be a hole or missing electron in the crystal structure. This hole will behave like a quasi-free positive charge. Therefore, these materials are know as P-type semiconductors.

4. Abrupt P - N Junctions

Alternate doping of adjacent regions of a single semiconductor sample can be used to form regions of excess electrons (N-type) and holes (P-type), with a sharp transition zone between the two regions. This discontinuity between the two materials is referred to as an abrupt P-N junction.

The abrupt P - N junction characteristics of semiconductor materials is exploited to create photovoltaic detectors. The energy band characteristics of a typical P - N junction are shown in Figure 2.2.
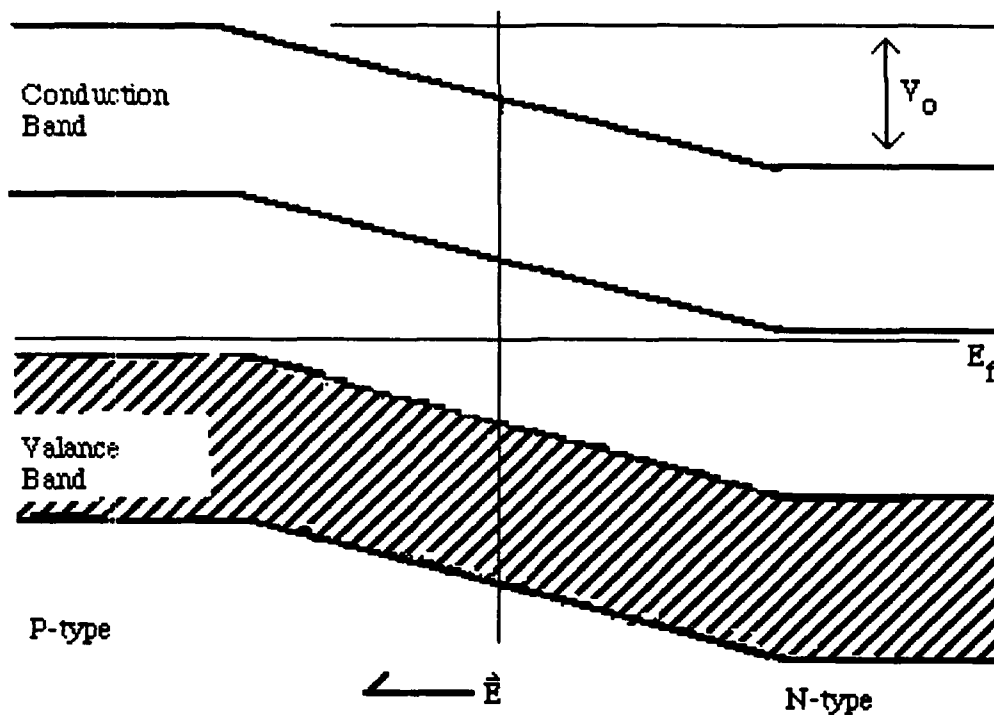
Figure 2.2 Abrupt P - N junction energy level diagram

This figure shows how the band gap energy of the material is changed in the area of the abrupt P - N junction. This transition occurs because of the discontinuous doping on either side of the junction. This produces a region where there are many fewer mobile charge carriers. Overall, this region is close to being neutrally charged. There are mobile charge carriers available, but their numbers are depleted. For this reason, the region near the abrupt junction is known as the depletion region.

In addition to a depletion region, a built-in electric potential difference is also created between the P and N regions. The presence of free electrons on the N region side and free holes on the P region side creates an electric field across the depletion region, as indicated by the direction of $\vec{E}$ in Figure 2.2. This, in turn, causes a space-varying electric potential that shifts the valence and conduction band potentials across the depletion region

by an amount V_0. It is seen in Figure 2.2 that the band gap energy remains essentially constant across this region, thus maintaining a continuous, albeit varying band gap across the junction. When a P - N junction is created, any free charge carriers migrate in response to the junction electric field until an equilibrium charge distribution is established.

In such equilibrium, with no externally applied bias voltage, there is no net average current flow in the P - N junction. However, if an electron - hole pair is created in the region then a current flow does result, because these new charge carriers will respond to the local electric field. An photon incident on the depletion region creates an electron - hole pair. The energy (hv) of a photon incident on this region must be greater than or equal to the band gap energy of the semiconductor material. This places a long wavelength limitation on the spectral response of the material. Likewise, the short wavelength limit is governed by the combined widths of the band gap and the conduction band. Figure 2.3 shows the spectral response of some common photovoltaic detectors.
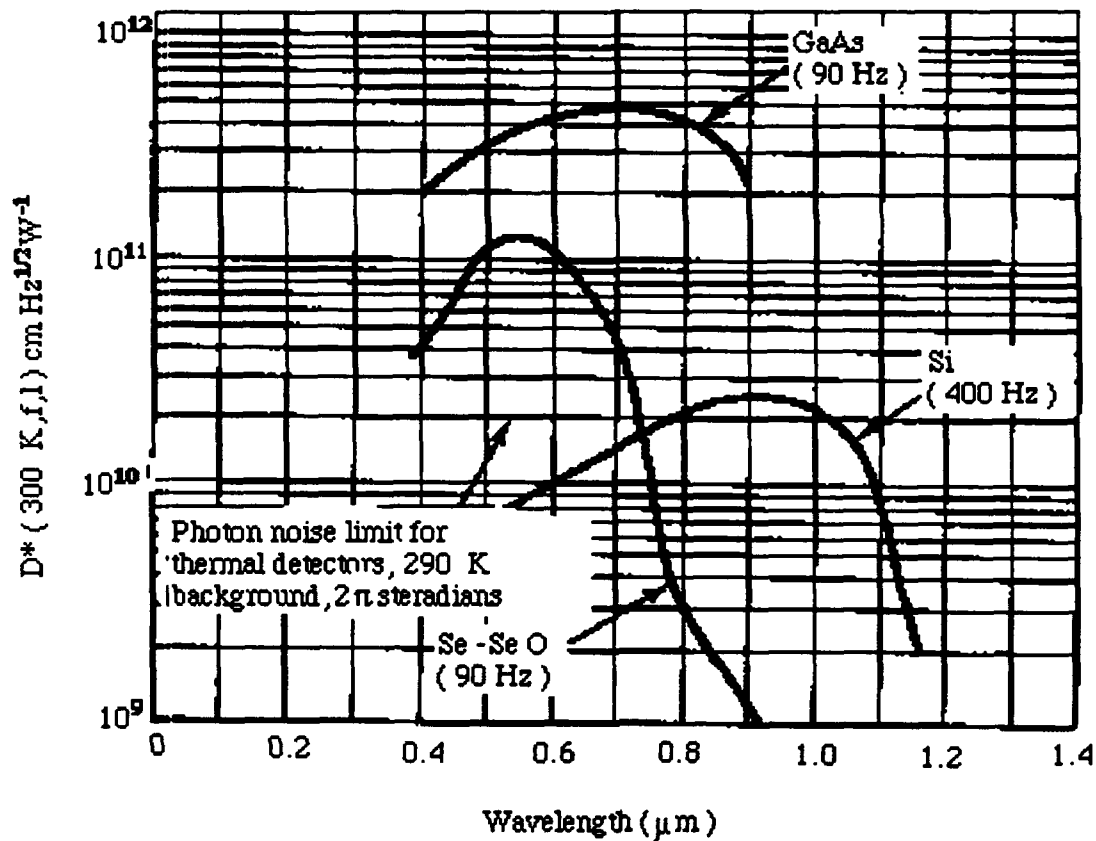
Figure 2.3 Photovoltaic diode spectral response characteristics

5. The Effects of Photon Flux in the Depletion Region

When the photon is absorbed in the depletion layer, a free electron - hole pair is produced in the material. The electron and the hole then move from the depletion region in response to the potential difference between the two regions. The electron tends to accelerate in the conduction band antiparallel to the local electric field and the hole accelerates in the valence band parallel to that field, causing a net current flow. This is the case in the P-N junction in Figure 2.4

Conduction Band

hv

Valance Band

P - Type $\vec{E}$ N - Type
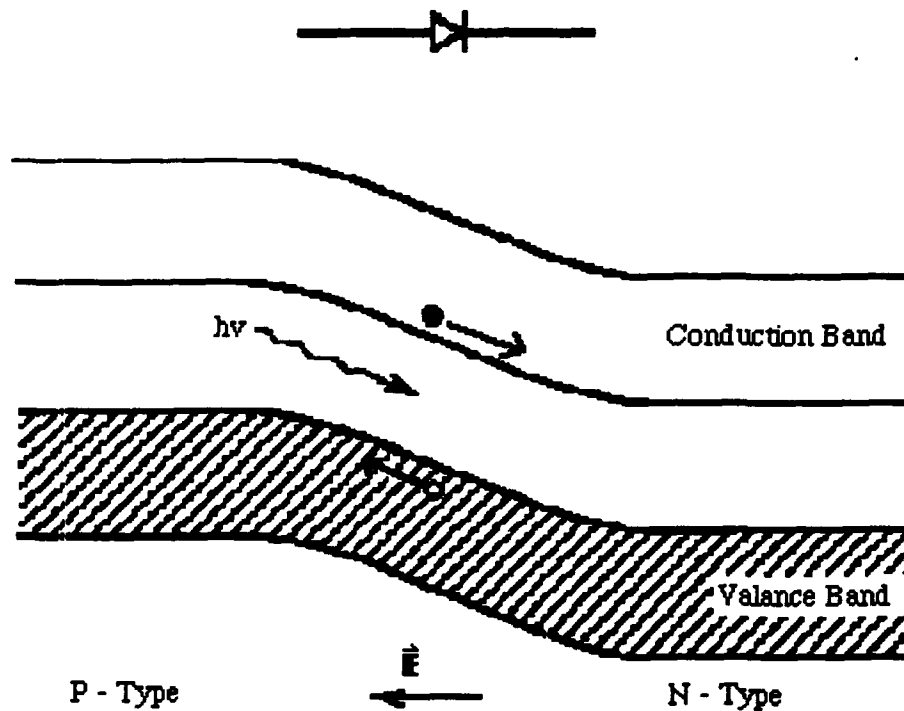
Figure 2.4 The absorption of a photon with energy hvin the depletion
region causing an electron - hole pair to be produced along with an
accompanying current flow.

The actual current can be calculated using the equation below (Boyd, 1983,

pg.189) as

$$i=\frac{-\eta eP}{hv}+i_{sat}(e^{(\frac{eV_a}{kT})}-1)$$

2.1

where η is the quantum efficiency (Boyd, 1983, pg.128), e is the electron charge, and P is

the power falling on the detector. The first term on the left side is the actual photocurrent

contribution and the second term is the Ebers-Moll contribution to the current from any

externally applied bias voltage (V_a) (Horowitz and Hill, 1989, pg.596). Figure 2.5 is a

graphical representation of this equation for various values of incident photon flux.

11

The rectifying characteristics of the detector also make it a useful diode. These characteristics can be plainly seen from Figure 2.5. The device is therefore often referred to as a photodiode and is denoted in schematic figures as a diode symbol.
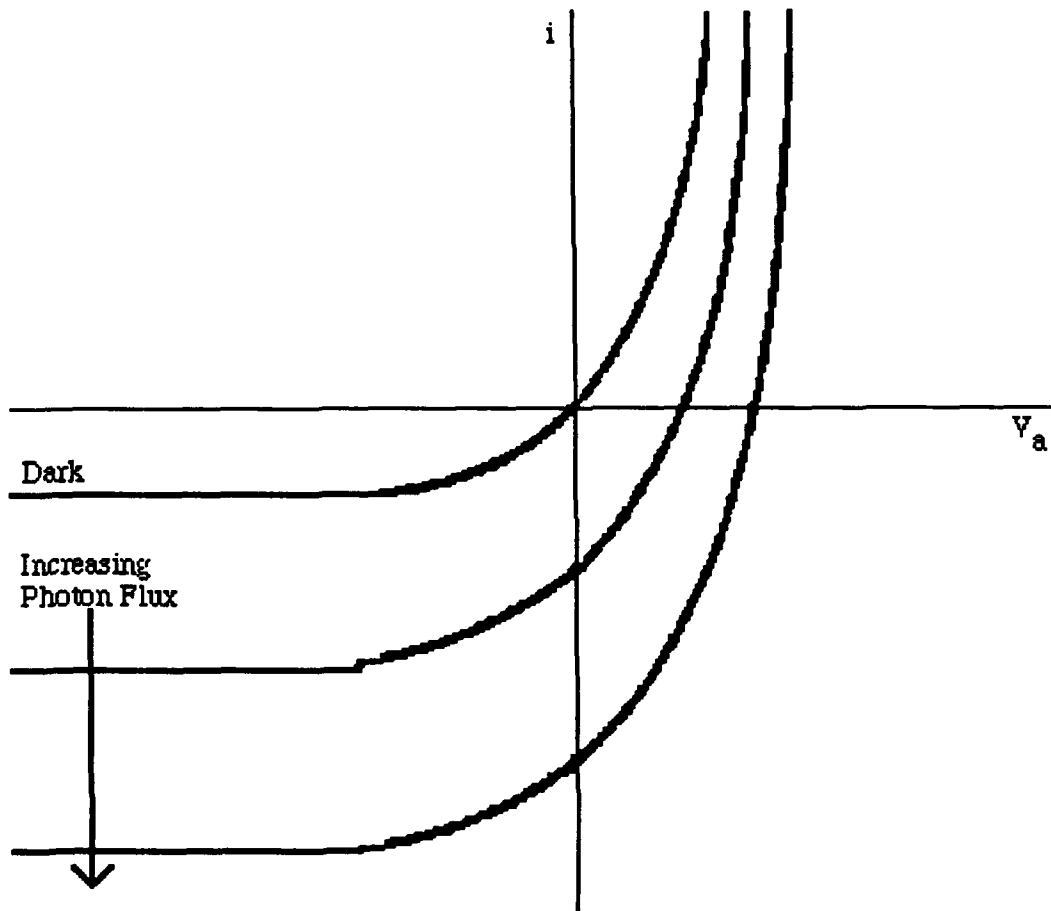
Figure 2.5 The current - voltage relation of a P - N junction exposed to various incident photon levels.

Whether of not there is an external voltage bias applied to a photodiode detector, the photocurrent measured at any fixed voltage level depends linearly on the optical power. It is this linear response that makes the abrupt P - N junction photodiode useful.

6. The Detector Characteristics

The characteristics of the actual detector used in the experimental portions of this thesis research were measured using techniques that are reported in Chapter VI. The effective detector resistance and impedance was measured using a Thevenin equivalent circuit that is described in detail in Chapter VI. The noise characteristics of the detector are also described in that chapter.

B. THE TRANSIMPEDANCE AMPLIFIER CIRCUIT

The direct use of a photovoltaic detector as a linear voltage source in an electronic circuit is not practical, because the device is a current source. The best generate only a few microamps of current, even with the most energetic incident light source.

In order to produce a usable linear voltage output from the detector it must be combined with an appropriate current-to-voltage converting amplifier. A transimpedance amplifier is used to provide the needed amplification and current-to-voltage characteristics of the detector circuit.

1. Basic Circuit Elements

The basic transimpedance amplifier, as shown in Figure 2.6, consists of only two additional components: an operational amplifier (opamp) and a feedback resistor .
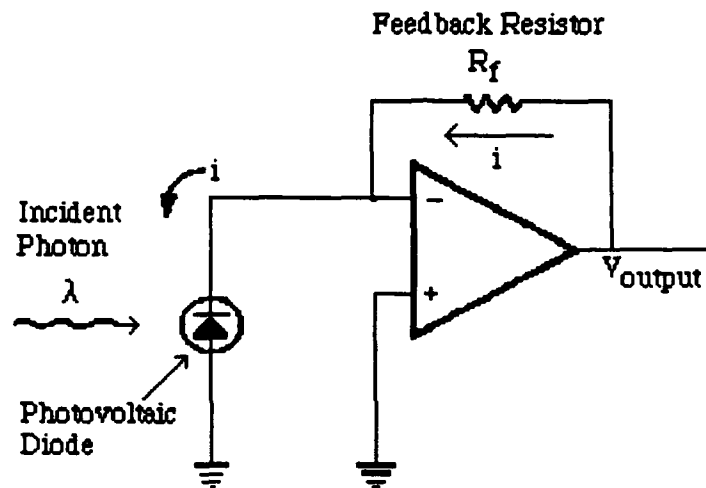
Figure 2.6   Basic transimpedance amplifier circuit

The basic operation of opamps and their characteristics are detailed in any basic electronics book (Horowitz and Hill, 1989, pp.175-177). The specific opamp used in this thesis is the LF412C, the characteristics of which are described by the manufacturer (Texas Instruments, 1992, pg.2.11 to 2.15).

2. Transimpedance Amplifier Operation

The noninverting input of the opamp is grounded. The inverting input is connected to both the input signal from the photovoltaic diode and to the feedback resistor. From the golden rules of opamp operation (Horowitz and Hill, 1989, pg.177), we see that the opamp in a negative feedback circuit will do whatever is necessary to its output to match the voltages at its inverting and noninverting inputs. The noninverting input is grounded; therefore, the inverting input will be maintained at zero voltage. The current flowing toward the inverting input from the photodiode must therefore be exactly matched by an opposite current flowing through the feedback resistor (R_f). There will also be no current flow into the opamp as stated in the same "golden rules".

14

Since the photocurrent flowing through the detector is i, which flows away from the opamp's inverting input in Figure 2.6, it follows that the feedback current must be an equal i flowing toward the inventing input. But the voltage at the inverting input is identically zero. Therefore, Ohm's law requires that

$$V_{output} - 0 = i\ R_{Feedback}\ ,\ or$$
$$V_{output} = i\ R_{Feedback} \qquad\qquad 2.2$$

with i being the current given by Equation. 2.1. Hence the ideal transimpedance amplifier produces an output voltage that is linearly proportional to incident monochromatic optical power.

III. OPTICAL / INFRARED BACKGROUND SIGNALS

In infrared observations, particularly those in the $2.5 \leq \lambda \leq 20$ μm region, ambient thermal radiation is the major contributor to both background signals and noise in the detection process. This background thermal radiation results from the finite temperature of the objects in the environment.

A. REVIEW OF THERMAL BLACKBODY RADIATION

An ideal blackbody is both a perfect absorber and a perfect emitter of radiation. The ideal absorber is one that absorbs all incident radiation, regardless of wavelength, angle of incidence, or polarization. A perfect absorber is obviously black since all visible radiation (light) is absorbed, hence the name blackbody to describe a perfect absorber. This is an ideal situation that can only be approximated by actual objects. A direct result of a body being an ideal absorber of radiation is that the body will also be an ideal emitter of radiation. This assumption about the relationship between the ideal absorber is proved by Kirchhoff's law (Kittel and Kroemer, 1980, pg.97) .

The perfect absorbing and emitting characteristics of the blackbody establishes the upper limit to the amount of radiation that can be emitted by any actual object. A perfect blackbody emitter can be approximated by a box or cavity which has a small hole in it. This small hole allows some of the radiation to escape without significantly changing the radiation field contained in the box; therefore the hole behaves like a blackbody.

The spectrum of the emitted radiation from a blackbody was explained by Max Planck in 1900 (Boyd, 1983, pg.39). The graphical representation of the Planck radiation law is shown in Figure 3.1. The figure shows the radiation spectral distribution at various absolute temperatures. The temperature dependance of the spectrum is such that, the higher the temperature, the higher is the spectral exitance at a given wavelength. The wavelength

16

peak of the exitance is described by the Wien displacement law (Boyd, 1983, pg.37) which is shown as the heavy dashed line in Figure 3.1.

The ambient temperature for objects at the earth's surface lie typically in the 275 - 300K range. The Wien displacement law, therefore, shows that the peak of the curve for typical temperatures encountered is in the infrared, at roughly $\lambda = 10\,\mu m$. The radiation is produced at a significant level over a much larger portion of the spectrum. Consideration of the properties of this unavoidable background radiation is therefore important when trying to measure a target by means of infrared sensing.

The spectral exitance of an actual radiator is always, by definition, less than that of the ideal blackbody radiator. The ratio of the actual exitance to the ideal blackbody's exitance is called the emissivity (Kittel and Kroemer, 1980, pg.97). The actual spectral emissivity is always less than unity. The actual radiator can therefore contribute significant radiation with emissivities that are significant.
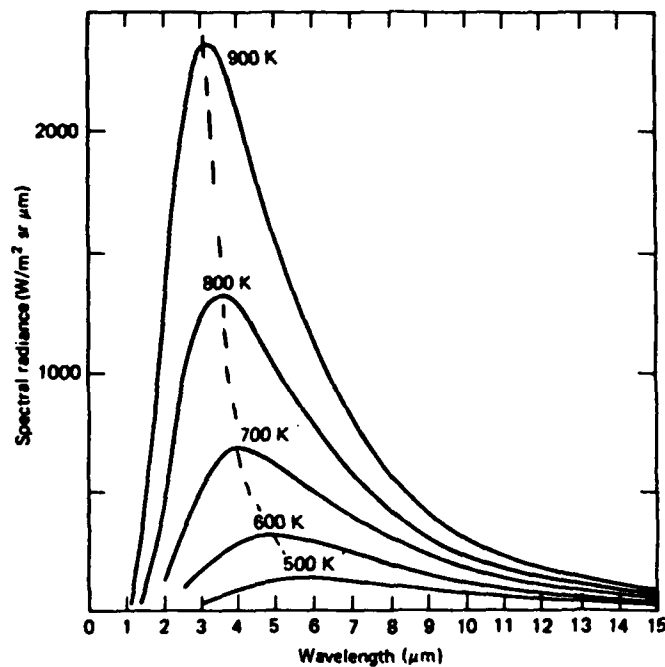
Figure 3.1 Graphical representation of Plank radiation law for various temperatures of interest. The Wein displacement law is shown as the dashed line through the peaks of the curves.

B. THERMAL BLACKBODY NOISE

The infrared radiation produced by a body as described in Section III A is quantized in the form of photons. The production and detection events for these photons are unpredictable in much the same way as are radioactive decays. Using simple statistical arguments, it can be shown from the Planck radiation law that the expected average number of photons incident upon a detector during any fixed interval and detector surface area is given by

$$\langle n \rangle = \frac{e^{-h\nu/kT}}{1-e^{-h\nu/kT}} \qquad 3.1$$

The noise fluctuation in the photon count is then calculated via the variance (Taylor, 1982, pg.86) in the usual manner:

$$\sigma_n^2 = \langle n^2 \rangle - \langle n \rangle^2 = \langle n \rangle \left[\frac{e^{h\nu/kT}}{e^{h\nu/kT}-1} \right] \qquad 3.2$$

For optical and infrared measurements, with $0.3 \leq \lambda \leq 30\mu m$ and $T < 1000$ K, $h\nu \gg kT$. It follows that

$$\frac{e^{h\nu/kT}}{e^{h\nu/kT}-1} \approx 1 \qquad 3.3$$

and so that

$$\sigma_n^2 \approx \langle n \rangle \qquad 3.4$$

Therefore, we may safely assume that, for infrared observations, with an average number of photons $\langle n \rangle$ striking the detector per second that the fluctuation, or noise, will be

$$\sigma_n = \sqrt{\langle n \rangle} \qquad\qquad 3.5$$

Therefore, the expected signal - to - noise ratio in the detection process will be

$$\frac{\langle n \rangle}{\sigma_n} = \sqrt{\langle n \rangle} \qquad\qquad 3.6$$

IV. SOURCES OF NOISE IN THE DETECTION PROCESS

In Chapter III, the quantized nature of electromagnetic radiation (i.e. photons) was shown to lead to the production of noise or a fluctuating electromagnetic field. This quantum nature gives rise to two noise contributions in a detected signal: (1) noise produced by the target of interest, and (2) noise generated from the flux of extraneous photons from the environmental background. Both of these noise sources would be present even if there were no additional noise contributions from the detector and its associated electronics. However, there are additional detector-specific noise sources.

Since the goal of this thesis has been to investigate the potential improvements to be gained from a new type of transimpedance detector system, it has been a major concern of this project to evaluate the noise characteristics of the conventional transimpedance detector system in order to insure that any modifications do not detract from the overall noise contributions to the detection process.

A. SOURCE NOISE

The discussions of Chapter II showed that the output voltage of a conventional photovoltaic transimpedance detection system is given by

$$V_{output} = R_f i_d \qquad 4.1$$

where R_f is the feedback resistance and i_d is the photocurrent through the detector. In Chapter III, it was argued that the rate at which photons arrive at the detector fluctuates in such a way that

$$\sigma_n = \sqrt{\langle n \rangle} \qquad 4.2$$

20

where σ_n is the RMS fluctuation and <n> is the average number of photons arriving at the detector during a defined time interval ΔT. It can be shown, in fact, that the statistical behavior of the photon flux obeys a Poisson distribution (Taylor, 1982, pg.208) , and that Equation 4.2 is a simple consequence of this statistical behavior.

The photoelectric behavior of the photovoltaic diode demands that an absorbed photon produce an electron - hole pair at the diode's junction. Therefore, if the average arrival rate of photons during an interval ΔT is

$$\frac{\langle n \rangle}{\Delta T}$$

4.3

it follows that the average photocurrent will be

$$\langle i_d \rangle = \frac{\langle n \rangle e}{\Delta T}$$

4.4

with $e = 1.60 \times 10^{-19}$ C as the fundamental unit of charge(Taylor, 1982, pg.208). But, <n> is not a constant value in time and will fluctuate as described by Equation 4.2. Therefore, i_d will fluctuate accordingly, producing a noisy photocurrent in the detection network.

As a consequence of this, a target will generate photon noise and an average signal level. This noise level will be described by Poisson statistics. The signal - to - noise ratio (SNR) associated with this fundamental quantum detection limit will be proportional to the square root of the target's average photon production rate. When bright targets are observed so that noise in the detection process is completely dominated by this behavior, the detection is said to be *source noise - limited*. This represents an absolute upper limit to overall SNR in any photon detection process.

B. BACKGROUND NOISE

The statistical description of background noise is completely analogous to that for source noise; the only difference is that the detected photons are generated by extraneous, and unwanted, sources. Typical background sources are the thermal blackbody radiation in the infrared region or reflected sunlight in the visible region.

When a weak target is observed against a bright background, as is usually the case in infrared observations, the background photon noise can completely dominate any other noise source in the system. Such a detector is said to be *background noise - limited.*

C. SHOT NOISE

Shot noise is the result of the photocurrent manifestation of the quantum behavior of the radiation field: a fluctuating photon arrival rate generates a corresponding fluctuating photocurrent. The variance in the photocurrent σ_{i_d} can be calculated in the usual manner (Taylor, 1982, pg.86) as

$$\sigma_{i_d}^2 = \left\langle \left(i_d - \langle i_d \rangle\right)^2 \right\rangle . \qquad 4.5$$

Using Equation 4.4, it follows that

$$\sigma_{i_d}^2 = \left\langle \left(\frac{ne}{\Delta T} - \frac{\langle n \rangle e}{\Delta T}\right)^2 \right\rangle = \frac{e^2}{(\Delta T)^2} \left\langle \left(n - \langle n \rangle\right)^2 \right\rangle \qquad 4.6$$

From Poisson statistics,

$$\left\langle \left(n - \langle n \rangle\right)^2 \right\rangle = \langle n \rangle \qquad 4.7$$

Therefore, by substitution

$$\frac{e^2}{(\Delta T)^2} \left\langle \left(n - \langle n \rangle\right)^2 \right\rangle = \frac{e^2}{(\Delta T)^2} \langle n \rangle \qquad 4.8$$

So it follows that

$$\frac{e^2}{(\Delta T)^2}\langle n \rangle = \left(\frac{e}{\Delta T}\right)\left(\frac{e\langle n \rangle}{\Delta T}\right) = \frac{e}{\Delta T}\langle i_d \rangle \qquad 4.9$$

This result is usually written in different form, using Nyquist's theorem (Kittle and Kroemer, 1980, pg.100). That is, if photons are detected for a time interval ΔT; the frequency spectrum of their arrival rate will be bandpass -limited to a finite frequency bandwidth Δf such that

$$\Delta T = \frac{1}{2\Delta f} \qquad 4.10$$

Hence, Equation 4.9 becomes

$$\sigma_{i_d}^2 = 2e\langle i_d \rangle \Delta f$$

or,

$$\sigma_{i_d} = \sqrt{2e\langle i_d \rangle \Delta f} \ . \qquad 4.11$$

This fluctuating shot noise current is produced by both the source photon noise and independently, by the background photon noise. Since the two sources are statistically independent, their shot noise currents must be added in quadrature(Taylor, 1982, pg.73) to predict the net shot noise in a given detector system.

D. JOHNSON NOISE

Unlike the noise sources described above, Johnson noise is not a consequence of any overtly quantized process. Rather, it arises because of density fluctuations of the charge carriers (usually electrons) in resistive circuit components (Boyd, 1983, pg.136). These density fluctuations are temperature (T), resistance (R) and measurement bandwidth (Δf) dependent. The resulting noise current is found to be

$$\sigma_i = \sqrt{\frac{4kT\Delta f}{R}} \qquad\qquad 4.12$$

E. 1/F NOISE.

In many classes of electronic circuits there is also found to be a peculiar and poorly understood extraneous noise, called *1/f noise* . The name derives from the approximate shape of the noise power spectrum. In electro - optical detection systems, 1/f noise is usually minimized by performing observations at frequencies sufficiently high so that 1/f noise is much smaller than that from the other sources. Hence, it can be neglected.

F. NOISE IN THE CONVENTIONAL TRANSIMPEDANCE SYSTEM.

The conventional transimpedance detection system (see Figure 2.6) consists of three components: the photovoltaic detector, the opamp and the feedback resistor. The detector itself is the generator of three noise currents: intrinsic Johnson noise (because the device has both finite temperature and resistance), shot noise induced by the target signal, and shot noise induced by the background. If these three noise currents are represented respectively by σ_{i_dJ} , σ_{i_dT}, and σ_{i_dB}, then the overall noise current σ_{i_d} from the detector will be expected to be given by

$$\sigma_{i_d}^2 = \sigma_{i_dJ}^2 + \sigma_{i_dT}^2 + \sigma_{i_dB}^2 \qquad\qquad 4.13$$

The opamp exhibits an intrinsic noise, which arises from a voltage, or alternative current, fluctuation at its inputs. Generally, opamp noise figures - of -merit are specified by the manufactures of such devices. For purposes of this thesis research, the chosen opamps have noise figures so low that their contribution to overall system noise is negligible. This will be shown for the actual circuit in the first section of Chapter VI. The feedback resistor's Johnson noise contribution, however, is not negligible.

The inverting input of the opamp is a virtual ground only to the extent that it forms a perfect current summing junction, with the sum of the currents identically zero. Independent noise currents from the detector and the feedback resistor will violate this condition; there will be a net noise current fluctuation

$$\sigma_{i_{total}}^2 = \sigma_{i_dJ}^2 + \sigma_{i_dT}^2 + \sigma_{i_dB}^2 + \sigma_{i_dR}^2 \qquad 4.14$$

at the summing junction. This will be amplified by the system to produce an output voltage noise of

$$\sigma_v = R_f \, \sigma_{i_{total}} \qquad 4.15$$

G. POSSIBLE IMPROVEMENTS TO THE TRANSIMPEDANCE SYSTEM.

Expanding the four terms of Equation 4.14 shows that all four terms have a noise current that is proportional to $\sqrt{\Delta f}$. This implies that it might be possible to improve the system design and suppress the noise level by restricting the transimpedance amplifier to operation across only a narrow frequency bandwidth. This assumes that the band center frequency is high enough to ignore the $1/f$ noise sources. This approach has been adopted for the new transimpedance system configurations studied in this thesis research.

V. AN EXTENDED TRANSIMPEDANCE DETECTION SYSTEM TO ADDRESS THE SATURATION PROBLEM

In the introduction (Chapter I) to this thesis, it was pointed out that the objective of this research has been to develop a transimpedance amplifier based detection system with improved performance by rejecting saturation due to high background noise levels. The standard transimpedance amplifier based detection system was subject to saturation because the opamp would saturate, not because the photodiode saturates in the optoelectronic sense. Even in the presence of large background photon fluxes, a typical photodiode still has plenty of dynamic range left.

The attempts to achieve an improved design had the following objectives and constraints: (1) to develop a system with enhanced sensitivity for a modulated target in the presence of unmodulated background; (2) to simultaneously ensure that the new design had improved noise characteristics at the target modulation frequency, and (3) to measure the actual performance characteristics of the resulting design.

A. THE BASIC DESIGN APPROACH

The basic idea for an improved design is stated simply. If the feedback resistor (R_f) in the conventional transimpedance amplifier is replaced by a complex, frequency - dependent impedance, then the desired sensitivity enhancement at a specific target modulation frequency might be achieved. Of course, this requires that this new feedback impedance Z_f have a maximum amplitude at the target modulation frequency. Furthermore, since a frequency - dependent Z_f necessarily entails a phase shift, care must be taken to ensure that phase shifts in the feedback loop never exceed 90°, which would destroy negative feedback and lead to circuit instability and possible oscillations. The extended transimpedance amplifier detection system will look like Figure 5.1.
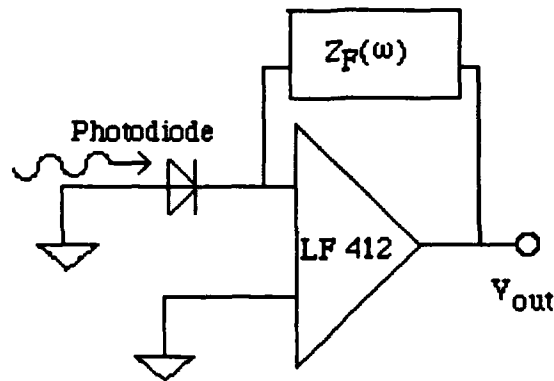
Figure 5.1 Extended transimpedance amplifier circuit with the frequency dependent impedance Z_F.

with the constraints that $|Z_F(f)|$ be a maximum at the target modulation frequency (f_o), and that real ($Re(Z_F)$) and imaginary ($Im(Z_F)$) portions of the signal be limited by

$$-90^\circ < \tan^{-1}\left(\frac{Im(Z_F)}{Re(Z_F)}\right) < 90^\circ$$

5.1

across the entire pass band of system operation.

B. DESIGN ATTEMPTS AND CONSIDERATIONS

Initial attempts were made using a conventional "tank" LC filters in combination with resistors to devise $|Z_F(f)|$.(Horowitz and Hill, 1989, pg.889) After several unsuccessful iterations, this approach was dropped when it was realized that LC circuits invariably yield insufficiently high $|Z_F(f)|$ at f_o when concomitant low $|Z_F(f)|$ at frequencies not equal to f_o is established.

The circuit design that can address this problem is the familiar compound RC filter known as a twin-T.(Horowitz and Hill, 1989, pp.279-281) In its basic form, it looks like Figure 5.2.
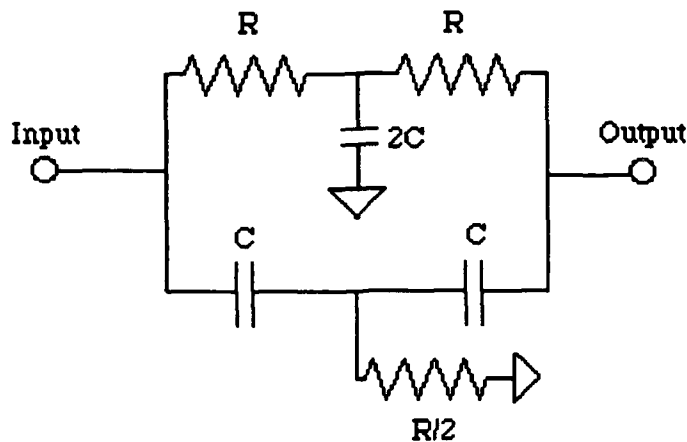
Figure 5.2   Basic twin-T circuit with matched resistors and capacitance.

When component values are chosen to be closely matched, this circuit exhibits extremely high impedance at $f = f_0$ and low impedance at f not equal to f_0, with

$$f_0 = \frac{1}{2\pi RC}$$

5.2

This twin-T approach, with $f = f_0 = 1.640$ kHz was adopted for this thesis work.

Extensive evaluation of transimpedance systems with basic twin-T included as the circuit feedback impedance Z_f revealed an intrinsic flaw in such a simple system. Invariably, these circuit networks produce pronounced phase shifts near f = fo. These phase shifts are large enough to violate the conditions put forth in Equation 5.1. This caused sporadic oscillation and severe noise in this circuit. These problems were addressed by an ad hoc combination of theoretical models and prototyped circuits, which are described in the following chapter.

VI. EXPERIMENTAL RESULTS

A. INTRINSIC NOISE IN THE CONVENTIONAL TRANSIMPEDANCE AMPLIFIER DETECTION SYSTEM

As stated in Chapter V, any proposed improved detector design is constrained to have noise characteristics that are no worse than those of conventional detector systems. Therefore, the quantification of the noise characteristics of a conventional transimpedance amplifier was necessary to establish a baseline for comparison with any improved circuit design.

The opamp chosen for this thesis research was the LF 412C. The LF 412C is a dual JFET input opamp with low offset and low drift. The unit is packaged as a standard dual in-line package. Additional technical specifications including noise characteristics are readily available (Texas Instruments, 1992, pp.2-11 to 2-15). The characteristics that make it desirable for this application are its high input impedance (on the order of 10^{12} ohms) and its low power requirements.

The resistor that was chosen for all initial noise measurements is a 2.2 megaohm (M) resistor. Two 2.2 M resistors were measured using a multimeter to have values of 2.23 M +/-.01 M. These resistors were placed in the circuit to form a basic transimpedance circuit as shown in Figure 6.1. The input resistor, R_i, is grounded to ensure that only the Johnson noise is measured in the circuit.

1. Lock-in Amplifier Operation

A lock-in amplifier was used to measure the output noise voltage from the circuit. This is not the only use for a lock-in amplifier, however. A lock-in amplifier is used to give an amplified output of a very weak voltage signal. When used to measure the voltage of an input signal the lock-in is capable of measuring noise down to the picovolt range. It is capable of making accurate measurements of an input signal even in the presence of high

noise levels. "Essentially, a lock-in is a filter with an arbitrarily narrow bandwidth which is tuned to the frequency of the signal. Such a filter will reject most unwanted noise to allow the signal to be measured." (Stanford Research Systems, 1989, pg.25) .

In addition to rejecting unwanted noise a lock-in can be used to measure the noise over a narrow bandwidth at a given reference frequency. The bandwidth of the noise is called the effective noise bandwidth or ENBW. This bandwidth has been identified as Δf in all the noise equations given in this chapter. For all noise measurements reported in this thesis, the lock-in amplifier output was consistently measured at various frequencies with a 1 Hz ENBW. The lock-in amplifier used to make these measurements is a Stanford Research Systems Model SR 510 Lock-in Amplifier.

2. Intrinsic Noise in the Amplification System without a Photodetector

The total noise is measured at the output of the opamp. The three sources of the noise in this circuit are Johnson noise of the two resistors and the intrinsic noise of the opamp itself. The specifications for the LF412 give an equivalent noise current of 1×10^{-14} A at 1000 Hertz (1 kHz) and a 1 Hz ENBW. This is the designed specification of the opamp which will be used to compare with the actual measured noise.
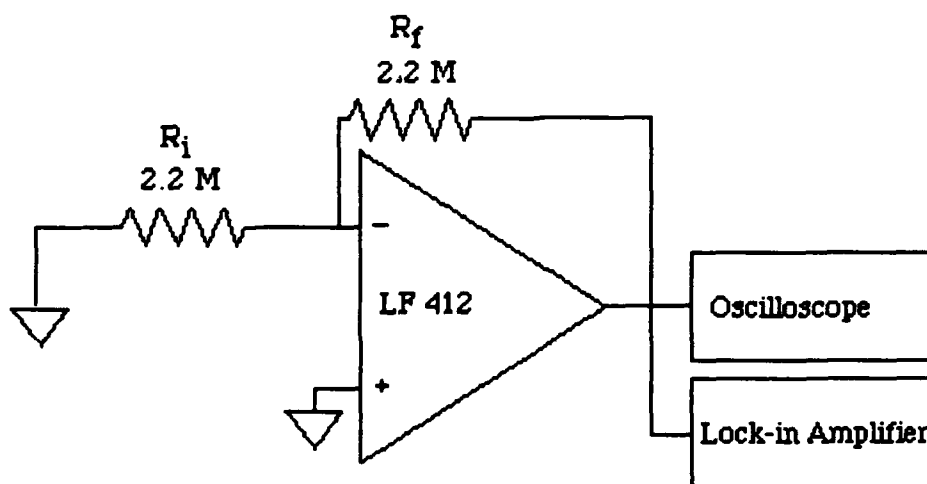

Figure 6.1 Basic transimpedance circuit without photodetector.

The first step was to measure the actual equivalent noise current for this circuit. The Johnson noise from a resistor, as you recall from Chapter IV, is given as

$$\frac{\sigma_{V_dJ}}{\sqrt{\Delta f}} = \sqrt{4kTR}$$

6.1

The equation for the relationship between the voltage and the current in this circuit is given by assuming that all current in the circuit passes through the feedback resistor. The Johnson noise current is given by a simple relationship as

$$\frac{\sigma_{i_dJ}}{\sqrt{\Delta f}} = \frac{\sigma_{V_dJ}}{\sqrt{\Delta f}\ R} = \sqrt{\frac{4kT}{R}} .$$

6.2

The equation for the total noise current in the circuit is therefore given by

$$\sigma_{i_dtotal}{}^2 = \sigma_{i_dopamp}^2 + \sigma_{i_{R_i}}^2 + \sigma_{i_{R_f}}^2 .$$

6.3

From this, the expected opamp noise ($\sigma_{i_dopamp}^2$) can then be determined the using equation above and setting $R_i = R_f = R$ as

$$\frac{\sigma_{i_dopamp}}{\sqrt{\Delta f}} = \sqrt{\left(\frac{V_{out}}{R}\right)^2 - \frac{8kT}{R}} .$$

6.4

The absolute temperature T was assumed to be room temperature or 300 K. Resistor values were chosen to match the dynamic resistance of the photodiode. The actual values of opamp noise current were then compared to the manufacturers specification of $1 \times 10^{-14} A/\sqrt{Hz}$. The measured noise current and the ratio of the measurements to manufacturers specifications are given in Table 6.1

## TABLE 6.1 RATIO OF DESIGN TO ACTUAL OPAMP NOISE CURRENT.

Frequency (Hz)	Actual $\sigma_{i_{opamp}}$	Design $\sigma_{i_{opamp}}$	Actual/Design
100	6.13×10^{-13} A/√Hz	1×10^{-14} A/√Hz	61.3
500	7.58×10^{-14} A/√Hz	1×10^{-14} A/√Hz	7.58
1000	1.06×10^{-13} A/√Hz	1×10^{-14} A/√Hz	10.6
5000	1.19×10^{-13} A/√Hz	1×10^{-14} A/√Hz	11.9
10000	1.06×10^{-13} A/√Hz	1×10^{-14} A/√Hz	10.6

As can be seen from these results, the actual noise values obtained for this circuit are an order of magnitude greater than expected between 500 Hz and 10 kHz. Below this range the 1/f noise seems to be a major contributor and the actual noise level was significantly higher. There are additional peaks at 60 and 120 Hz which suggests that AC power line sources are radiating into the circuits increasing the noise level by a factor of 1000 at those frequencies.

3. The Total Noise Contribution of the Photodiode

The noise characteristics of the purely electronic components having been established in the previous section, we can continue to quantify the noise associated with the photodiode. The input resistor is replaced by the photodiode in the circuit as shown in Figure 6.2. The photodiode is shielded from all external photon sources to significantly reduce any current flow in the circuit due to photoelectron current flow.
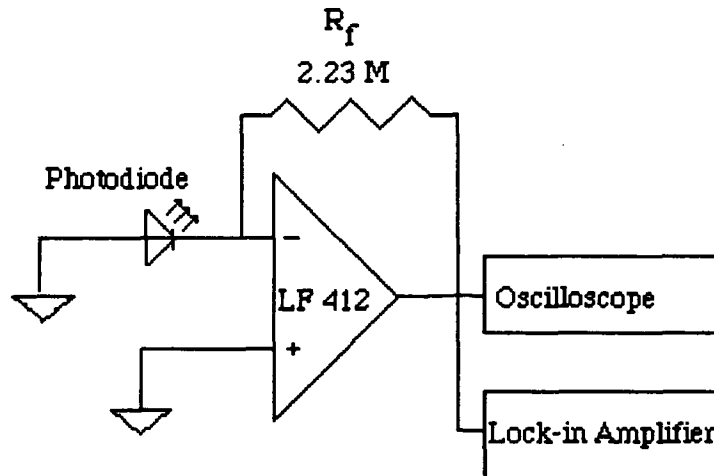
Figure 6.2 Circuit with photodetector replacing the input resistor.

The lock-in amplifier and oscilloscope are then connected to the output of the circuit, and the output voltage is measured . The three noise sources in the circuit are the feedback resistor, the opamp and the photodiode. These noise sources are all again assumed to be independent of each other and therefore they all add in quadrature to produce the total noise. The equation for the total noise then becomes

$$\sigma_{i_{total}}{}^2 = \sigma_{i_{opamp}}^2 + \sigma_{i_{detector}}^2 + \sigma_{i_{R_f}}^2 \ .$$

6.5

Again, all the current is assumed to pass through the feedback resistor. Therefore, the total noise current can be calculated as above. Substituting into Equation 6.3 and solving for the noise generated by the photodiode gives

$$\frac{\sigma_{i_{detector}}^2}{\sqrt{\Delta f}} = \sqrt{\left(\frac{-4kT}{R}\right)^2 + \sigma_{i_{opamp}}^2 + \left(\frac{\sigma V_{out}}{R}\right)^2} \ .$$

6.6

The output noise voltage ($\sigma V_{out}/\sqrt{\Delta f}$) was then measured across the previously determined range of 500 Hz to 10 kHz. The noise current characteristics of the detector are

33

compiled in Table 6.2. The overall noise characteristics show a marked increase at frequencies above 5 kHz.

TABLE 6.2 CALCULATED PHOTODIODE NOISE CURRENT AT VARIOUS FREQUENCIES FROM OUTPUT NOISE VOLTAGE.

Frequency (Hz)	$\sigma_{V_{out}}$ ($\mu V/\sqrt{Hz}$)	$\sigma_{i_{detector}}$ ($A/\sqrt{Hz}$)
500	.30	2.55×10^{-14}
1000	.30	2.95×10^{-14}
2000	.30	2.95×10^{-14}
3000	.35	7.72×10^{-14}
5000	.35	7.72×10^{-14}
6000	.40	1.22×10^{-13}
7000	.40	1.22×10^{-13}
8000	.50	1.81×10^{-13}
9000	.50	1.81×10^{-13}

4. The Effective Resistance and the Johnson Noise of the Photodiode

Now that the effective noise level from the photodiode has been determined the photodiode effective resistance is measured to compare the Johnson noise produced by this resistance with the photodiode noise measured above. In order to measure the effective resistance an equivalent representation of the photodiode must be constructed. The photodiode Thevenin equivalent circuit, as shown in Figure 6.3, is an ideal voltage source in a parallel with capacitor, all in series with a resistor. This equivalent circuit has noise associated with the Johnson noise in the resistor ($R_{detector}$) and an intrinsic noise associated with the voltage source. The Johnson noise associated with effective resistance can be determined by indirectly measuring the effective resistance.
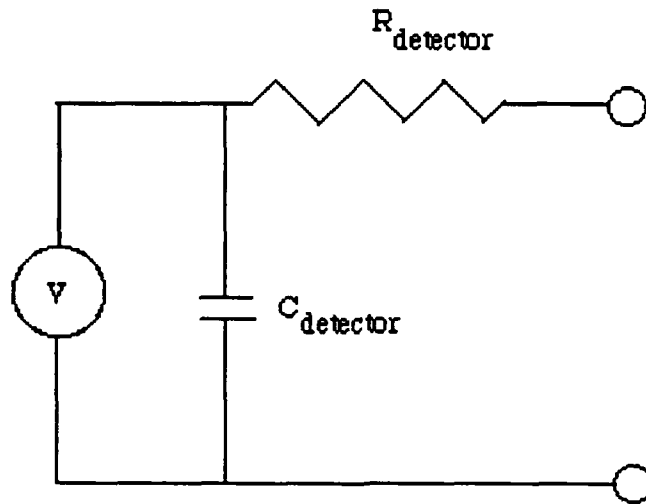
Figure 6.3 Thevenin equivalent circuit for the photodiode.

The current-voltage characteristics of the photodiode are covered in detail in Chapter II. For a photodiode with no incident flux the photodiode output will be similar to Figure 2.5.

The inverse slope of that graph is the effective, or dynamic, resistance of the photodiode (Horowitz and Hill, 1989, pg.44). The operating point of the photodiode will be within several millivolts and nanoamps of the origin. This is the range where we will determine the effective photodiode resistance. Across a small domain near the origin the current and voltage are almost linearly related. Therefore, the calculation of the effective resistance ($R_{detector}$) is given by

$$R_{detector} = \frac{\Delta V_{detector}}{\Delta I_{detector}} \qquad 6.7$$

The current flow through the circuit ($I_{detector}$ or I) cannot be measured directly, because it is so small. However, as shown in Chapter II, the transimpedance amplifier produces an output voltage that is a simple function of $I_{detector}$. See Figure 6.4 below.
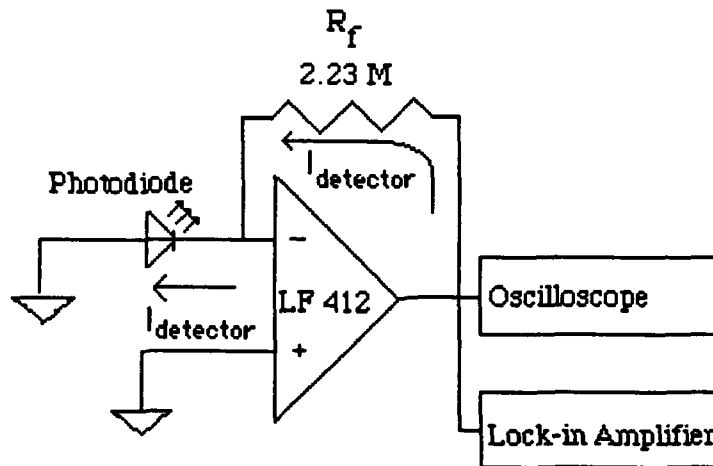
Figure 6.4 Current flow in the basic transimpedance amplifier.

There is no appreciable current flow through the opamp because of its high input impedance ($10^{12} \, \Omega$). The direction of current flow is determined by whether V_{out} is positive or negative. The current flow through the resistor can then be found as

$$I_{detector} = \frac{V_{detector} - V_{out}}{R_f} \qquad 6.8$$

The voltage V_{out} was measured accurately using a sensitive multimeter. The Philips PM2525 is a sensitive multimeter and has a precision of 10^{-6} V. The voltage $V_{detector}$ will be the same as that at the noninverting input of the opamp. This is due to negative feedback which always does whatever is necessary to make the voltage difference between the inverting and noninverting inputs of the opamp zero. Hence, $V_{detector} = 0$ ideally for the circuit in Figure 6.4. If the noninverting input is held at some other voltage, $V_{detector}$ will automatically match the new voltage. Measured values of V_{out} and $V_{detector}$ are compiled along with the calculated values of $I_{detector}$ in Table 6.3.

The effective resistance near the origin was then found using Equation 6.4. A variety of experiments were preformed using conventional silicon photodiodes. In all cases

the effective resistance was found to be of the order of 1 M +/- .1M . The effective

resistance for various current and voltages are listed in Table 6.3.

TABLE 6.3 CALCULATED DETECTOR CURRENT AND RESISTANCE.

$V_{detector}$ (mV)	V_{out} (mV)	$I_{detector}$ (nA)	$R_{detector}$ (M)
25.003	24.521	25.003	1.0
20.004	19.517	20.003	1.0
15.005	14.523	15.004	1.0
10.021	9.524	10.020	1.0
5.007	4.511	5.007	1.0
.008	-.484	.008	1.0
-5.003	-5.507	-5.003	1.0
-10.015	-10.522	-10.015	1.0
-15.002	-15.530	-15.002	1.0
-20.004	-20.526	-20.004	1.0

In order to determine the noise created by the photodiode's effective resistance,

we use the equation for Johnson noise current for a resistance. The equivalent Johnson

noise current created by the effective photodiode resistance can be calculated as

$$\frac{\sigma_{i_{detect}}}{\sqrt{\Delta f}} = \sqrt{\frac{4kT}{R_{detector}}} = \sqrt{\frac{4\times\left(1.38\times10^{-23}\right)\times300}{10^6}} = 1.28\times10^{-13} \text{ A}/\sqrt{Hz}$$

6.9

Remarkably, this value is in agreement with the detector noise current measured

in the previous section. The noise currents agree to two significant digits between six and

seven kilohertz and are within a factor of 10 for all other frequencies in Table 6.2. This

indicates that the Johnson noise source is the predominant noise source in the unilluminated

detector. There appear to be no additional noise contributions to the unilluminated detector.

Therefore, the levels actually measured for the total noise of this unilluminated system will

be referred to as the photodiode Johnson noise. This will be important when the circuit shot noise is measured with an incident photon source illuminating detector. The photodiode Johnson noise is assumed to be independent of the shot noise and unchanged with varying incident photon levels.

5. Shot Noise in the Detection Process

The Johnson noise exists in the circuit because of the finite photodiode resistance and temperature. The shot noise is a result of statistical fluctuations in the arrival times of photons, and the average DC photocurrent is proportional to the average photon flux. The circuit shown in Figure 6.2 was the same circuit used to measure shot noise. The detector was uncovered and exposed to the ambient photon flux.

As before, assuming that all the current flow will be all passing through the feedback resistor, the following is then the equation for the current

$$I_{detector} = \frac{V_{out}}{R_f} \qquad 6.10$$

For these experiments, the ambient light intensity was held constant, so that the DC component of V_{out} was maintained at 4.4 V. The feedback resistor was still 2.23 M. The DC component of the current (I_{dc}) was then calculated to be 1.97 x 10^{-6} A. The predicted shot noise was then calculated, using Equation 4.10, as

$$\frac{\sigma^2_{i_{shot}}}{\Delta f} = \sqrt{2eI_{detector}} = \sqrt{2 \times 1.6 \times 10^{-19} \times 1.97 \times 10^{-6}}$$

$$= 7.94 \times 10^{-13} \text{ A}/\sqrt{Hz} \qquad 6.11$$

In order to validate this result, the noise current in Equation 6.11 is contrasted with the shot noise derived for the same ambient light conditions, however, using the actual system noise measurements vice the DC current. The lock-in amplifier was used to

38

measure the actual noise output. The noise was measured at 10 kHz with a 1Hz ENBW . The total noise voltage was found to be 1.55 x 10^{-6} V/$\sqrt{Hz}$. Since the current is assumed to flow through the feedback resistor, the total noise current is then

$$\sigma_{i_{shot}} = \frac{\sigma_{v_{shot}}}{R_f} = \frac{1.55 \times 10^{-6}}{2.23 \times 10^{6}} = 6.95 \times 10^{-13} \text{ A/}\sqrt{Hz} \qquad 6.12$$

In summary, the sources of noise are: (1.)the Johnson noise current of the feedback resistor (1.34 x 10^{-14} Amperes/$\sqrt{Hz}$); (2.) the Johnson noise current of the photodiode (1.81 x 10^{-13} Amperes/$\sqrt{Hz}$); (3.) The intrinsic opamp noise current (1.06 x 10^{-13} A/$\sqrt{Hz}$). The expected shot noise contribution is then found to be

$$\sigma_{i_{shot}}{}^2 = \sigma_{i_{total}}{}^2 - \sigma_{i_{opamp}}^2 - \sigma_{i_{detector}}^2 - \sigma_{i_{R_f}}^2 \qquad 6.13$$

$$= \left(6.95^2 - 1.81^2 - 1.34^2 - 1.06^2\right) \times 10^{-26}$$

$$= 42.11 \times 10^{-26} \text{ A}^2/\text{Hz}$$

The expected total shot noise is therefore 6.49 x 10^{-13} A/$\sqrt{Hz}$. This is somewhat lower than the actual predicted contribution of the shot noise source in Equation 6.11. There appears to be an additional, unexplained, noise source (possibly electrical pickup, power supply noise, etc.) contribution to overall noise characteristics, but the bulk of the noise is explained successfully by known contributors. Therefore, we were confident that shot noise is the dominant noise source for this system.

B. DEVELOPMENT OF A TARGET SIGNAL GENERATING SOURCE

As a test source for new transimpedance system designs, we needed a stable, monochromatic source capable of being modulated at frequencies of up to 10 kHz. A

conventional GaAs yellow light emitting diode (LED) was chosen as the device to meet this need. It has a characteristic 1.2 V diode forward voltage drop.

1. A First Attempt at Producing a Source Signal

A circuit patterned after the design produced by Lt. Parriottt (Parriott, 1991, pg.10) was adapted, as shown in Figure 6.5. The circuit uses a 2N3904 transistor emitter follower to provide the current flow necessary to drive the LED.(Tower, 1989, pg.60) This transistor has a maximum collector current of 200 mA, which is more than sufficient for this circuit. The base is driven by a laboratory function generator. This provides a high driving current output without overloading the input signal source. In practice, this circuit produced an observable optical output signal with the LED. However, this output was nonlinear and was not as easily controlled as desired. Analysis of the circuit showed that it put an undue load on the frequency generator,despite the emitter follower buffer.
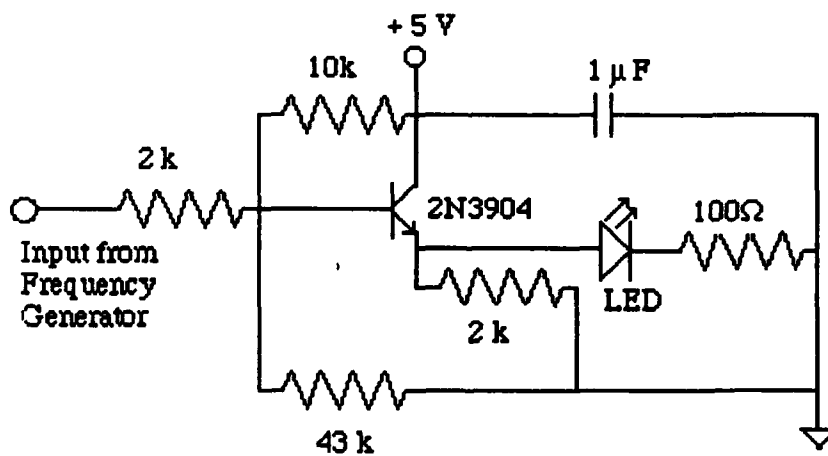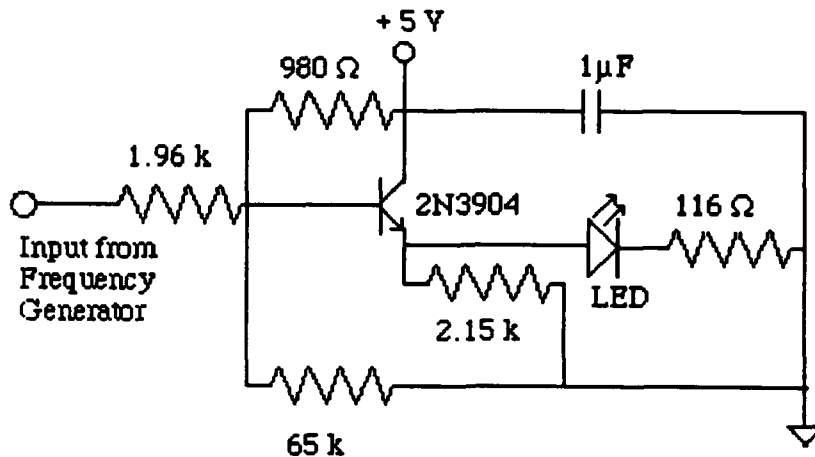

Figure 6.5 Adapted source LED circuit

2. The Final Modified Source Signal

The circuit was modified as shown in Figure 6.6. This circuit has a higher base voltage and has very little loading of the frequency generator. The circuit was operated at

40

all times at its optimum output which corresponded to a frequency generator output of 4.8 volts peak to peak and a 0.2 V offset voltage.

Figure 6.6 The final source LED circuit

This circuit produced a reproducible sinusoidal output from the LED when driven by a sinusoidal signal. Measuring the voltage level across the LED, the voltage varied sinusoidally between zero (or no current flow) and 1.3 Volts. The peak current was then found to be

$$I_{LED} = \frac{V}{R} = \frac{1.3V}{116\,\Omega} = 11.2\ mA \qquad\qquad 6.14$$

This is well below the maximum design current of the circuit and will provide a reproducible and well-defined target source to be detected against the background.

C. THE BACKGROUND SIGNAL SIMULATOR

The improved transimpedance detector system that is the design goal of this thesis project will have to detect modulated targets against intense, noisy backgrounds, as are typical in infrared (IR) applications. However, the simple systems investigated here operated in the visible spectral range. Therefore, in order to simulate the background produced by an IR environment, it was necessary to develop a simulator to provide

41

artificial background and noise (see Chapter III). An ideal simulator will produce a strong average background signal, modulated by a random fluctuation whose amplitude is equal to the square root of the average, thereby mimicking the Poisson statistical behavior of the real IR environment.

1. Initial Attempts at Simulator Development

As an initial attempt a 5 V DC incandescent lamp was used to generate a background source powered by a 6 V DC battery, as shown in Figure 6.7. This produced a strong simulated background level at the detector, but with very little noise. In an attempt to produce appropriate statistical fluctuations in the background level, a power MOSFET was placed in the circuit as shown in Figure 6.8, and the lamp power was varied using a random noise generator.
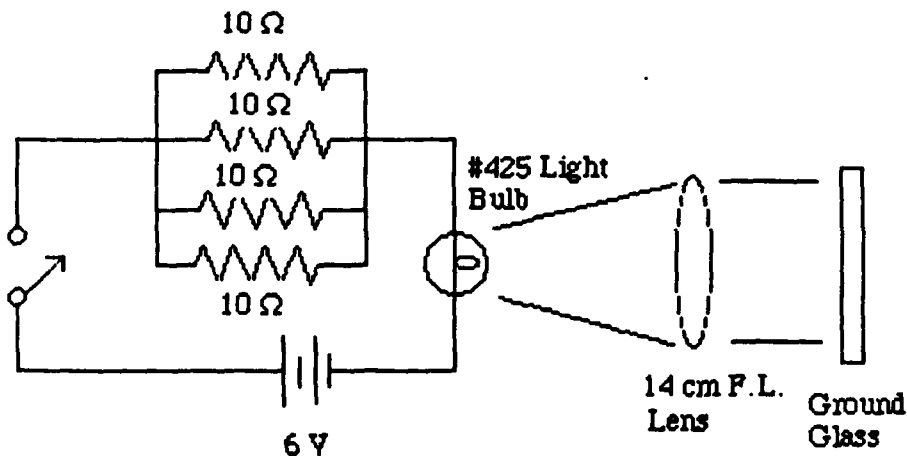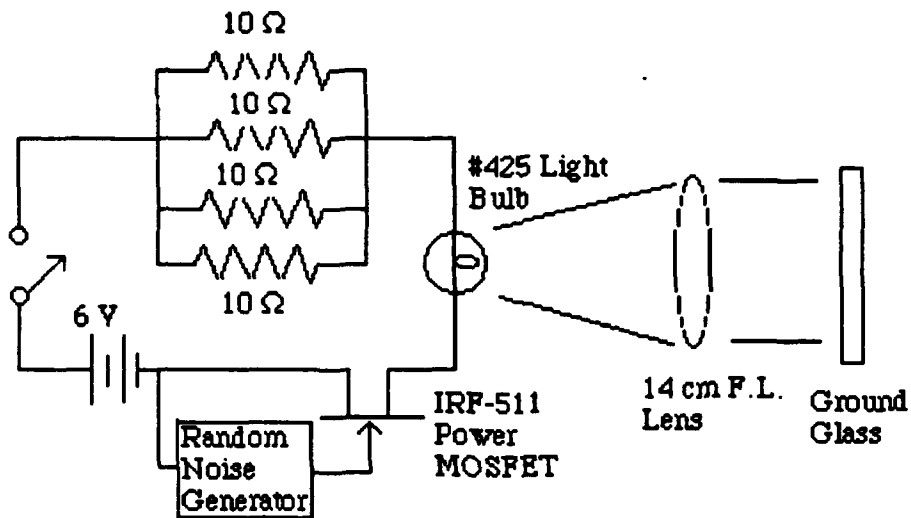

Figure 6.7 Basic background light source using a standard light bulb

Figure 6.8 Background light source with random input using Power MOSFET

This produced a varying light source, however the characteristic time constant of the lamp filament limited the frequency response of the circuit to only a few tens of Hz. It was obvious that the thermal heating and cooling rate of the filament controlled the frequency response of the system. The light was unable to respond at a frequency above 30 Hertz. This method is therefore not a valid method of simulating a background with a flat noise frequency spectrum at frequencies of interest.

2. LED-Based Background Simulator

In order to get the frequency response required for the simulator, another LED was chosen as the light source. The LED used must be able to produce a photon flux that created a detector output voltage on the order of several volts. The small LED used in the target circuit (see Section VI B) produced only a few microvolts output from the detector. This will not be a sufficient level for the background simulator.

The LED chosen for use in the background simulator is the Archer/ Radio Shack Jumbo Super Bright LED. This LED has a forward continuous current of 30 mA and a power output of 75 mW. It produces its peak emission at a wavelength of 660 nm, which

43

is in the visible (red) spectrum. This is capable of saturating the detector circuit when the LED is driven at its maximum power output.

This LED was placed in a circuit identical to that for the target signal generating source (see Figure 6.6) . The circuit was constructed initially with a sinusoidal frequency generator at the input instead of a random noise generator to check the frequency response characteristics of the LED and the circuit. The circuit and LED were able to reproduce faithfully a sinusoidal input as a sinusoidal detector output at frequencies up to 50 kHz . The circuit will therefore not limit the frequency response of the background simulator.

Using a HP 3561 spectrum analyzer as a random noise generator, this circuit was unable to produce an output fluctuation that was sufficiently strong to simulate a Poisson distribution.

To verify this observation, the output of the background LED was directed at the photodetector, where RMS voltage output was measured using a BK 2703 Multimeter. This gave a value of 601 millivolts for the average voltage. The detected RMS noise voltage to simulate a Poisson noise distribution should have been $\sqrt{601}$, or 24.5 mV. The actual detected noise was 1.5 millivolts, which is substantially less than the needed level.

3. A Summing Transconductance Amplifier for the Background Simulator Circuit

In order to increase the random noise produced from the input signal a new circuit was constructed, as shown in Figure 6.9. This circuit has several characteristics that make it ideal for use with the background LED. The input potentiometer gives the ability to adjust the noise level to correspond to the required level. The 1 M potentiometer is used to produce an offset voltage, which gives fine control over the LED's average output level. These two potentiometers together are used to produce a background output with the desired level of noise at a given frequency.
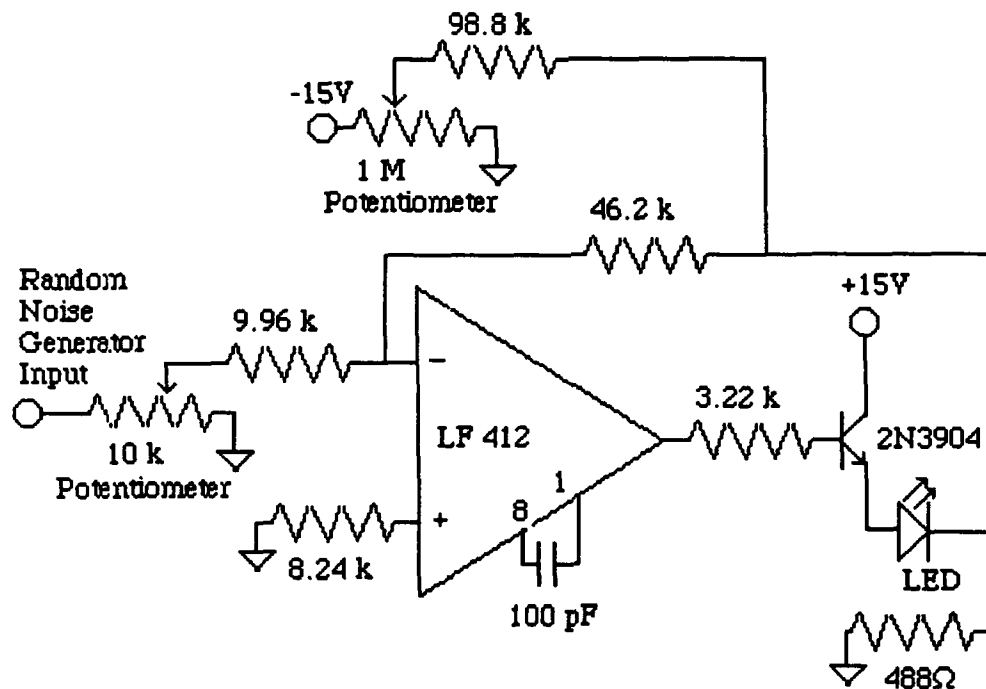
Figure 6.9 Transconductance amplifier-based background simulator

The background simulator was tested over the entire operating range from 500 Hz to 5kHz. The two potentiometers were adjusted at all frequencies to produce the desired Poisson distribution of the noise. Since the target will be modulated at a frequency f_o, this gives the circuit the ability to obtain a Poisson distribution at the modulated frequency. As an example, the potentiometers were set to produce a Poisson distribution at 2000 Hz. The noise levels were measured for a number of frequencies using the SR-510 lock-in amplifier. Table 6.4 shows the background noises and the RMS output of the LED at the detector.

TABLE 6.4 LED BACKGROUND RMS AND NOISE VOLTAGE MEASUREMENTS.

Frequency (Hz)	σ_v (mV)	V detector RMS (mV)
250	4.3	12.5
500	4.7	12.5
1000	4.0	12.6
2000	3.6	12.6
2600	3.3	12.6
3100	3.3	12.5
3700	3.2	12.5
4500	2.7	12.6
5000	3.0	12.5

D. INTEGRATED SYSTEM OPERATION WITH CONVENTIONAL TRANSIMPEDANCE AMPLIFIER CIRCUIT

1. The Optical Table

The background and source signal generators were mounted on the optical table with the detector circuit to determine the operational limits of the system. The optical table has many desirable properties that make it an ideal platform for measuring an optical source. The table is a stable, level platform that can isolate the table from external vibrations. The biggest drawback to the optical table is that the table top is made of a machined steel plate. This steel plate acts like a giant antenna and/or capacitor plate, which can interfere with operation of any electrical equipment. The electrical circuits all had to be isolated in individual metal boxes to prevent any electrical pick-up at the detector circuit due to the high gain of the detector system. The integrated system was placed on the optical table as shown in Figure 6.10.

46
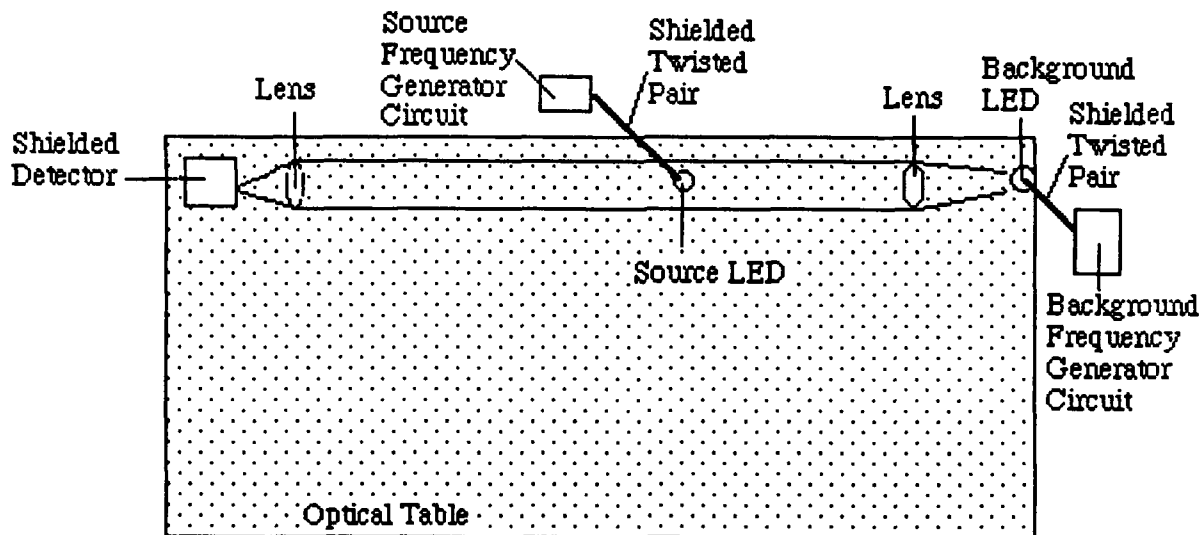
Figure 6.10 Overhead view of assembled detection system.

The shielded twisted pair shown in Figure 6.10 is a special type of cable for decreasing or eliminating unwanted radiation of electrical signals (Horowitz and Hill, 1989, pg.605). The lenses used were standard positive (converging) types with a focal length of 14 cm. The lens at the background simulator is placed so that its focal plane falls on the background LED. This ensured that the background photons are directed at the detector as a nearly collimated beam. The lens at the detector, however, has the photodiode located in its focal plane. This creates the largest possible signal for the detector circuit for both the source and the background light sources.

2. Conventional Detector System Response

The transimpedance detector system was assembled on the optical table as shown in Figure 6.10. The detector was modified to have 10 M feedback resistor. This gave the detector a greater sensitivity and a slightly higher intrinsic noise level due to the increased Johnson noise in the larger R_f. The overall circuit still only produced a noise voltage of 1.7 μV at 1kHz. The detector output was routed to both the lock-in amplifier and to an oscilloscope. The signal was carried between the detector box and these two instruments

47

with standard coaxial cables, since the use of a shielded twisted pair did not appear necessary. The cables ran directly away from the optical table and thus had minimal proximity to the table top and its potential detrimental effects.

a. No external signal

First, with no background or source on, that is with the detector covered, the system behaved as in Section VI A. The oscilloscope was able to detect a noise signal larger than a tenth of a mV, which is substantially larger than the few μV of intrinsic noise produced by the detector circuit. The lock-in was able to measure the noise voltage present in the covered detector as $0.4\ \mu V/\sqrt{Hz}$. This noise remained constant over the range of 500 Hz to 5000 Hz. These results are shown in Table 6.5 below.

b. Source LED only

The target source light was next used with no background. In order to ensure that no background light was present, these readings were taken at night. The oscilloscope showed that there was no stray light background level present at its 0.1 mV sensitivity level. The lock-in still indicated the presence of a $0.4\ \mu V/\sqrt{Hz}$ noise, just as it did when covered. The source LED was then modulated at a frequency of 500 Hz to 5kHz. The oscilloscope was unable to detect any change at the given modulation frequency. However, the lock-in was able to detect a signal at approximately $10 \mu V$. The actual detected signals are tabulated in Table 6.5 below.

c. Background and source LED's

The background and the source were both turned on. The background was adjusted to have an average voltage level of 16 mV and an RMS fluctuation equal to 4 mV. As expected, the conventional transimpedance system could not detect the target against the strong, noisy background, using either the oscilloscope or the lock-in. This is also shown in Table 6.5.

## TABLE 6.5 CONVENTIONAL TRANSIMPEDANCE DETECTOR RESPONSE TO THE TARGET AND BACKGROUND SIGNALS.

Frequency (Hz)	σ_v Detector only	V_{out} Target LED	V_{out} Both LED's
250	.4 μV	9.4 μV	<5μV
500	.4 μV	9.7 μV	<5μV
1000	.4 μV	9.8 μV	<5μV
2000	.4 μV	9.5 μV	<5μV
2600	.4 μV	9.6 μV	<5μV
3000	.4 μV	9.4 μV	<5μV
3700	.4 μV	9.6 μV	<5μV
4500	.4 μV	9.6 μV	<5μV
5000	.4 μV	9.8 μV	<5μV

E. THE BASIC TWIN-T CIRCUIT

The twin-T circuit, as described in Chapter V, was chosen as the frequency -dependent feedback impedance, Z_f. It is a circuit that requires precision matching of its components in order to develop a high Q , or a sharply peaked resonance. The resistance and capacitance were chosen so that the resonant frequency was between 1 and 5 kHz, which the earlier noise measurements (see Section VI A) indicated as the desired range for best response. The components were chosen from commercially available stock. Over 100 samples of each component were measured to achieve optimum matching. The components chosen all agreed to four significant digits for resistors and three significant digits for capacitors. Recalling from Chapter V that the twin-T has very high impedance at its resonant frequency and substantially lower at other frequencies. The resonant frequency for the chosen components is calculated as

$$f_0 = \frac{1}{2\pi RC} = \frac{1}{(2\pi)(99.06 \text{ k})(1.02 \text{ μF})} = 1.575 \text{ kHz}$$

6.15

This is the expected value assuming ideal circuit behavior. The actual impedance values were calculated indirectly from the current and voltage drop across the twin T and showed a slightly different resonance frequency. In order to take these measurements, the twin-T was treated as single frequency-dependent resistor ($Z(\omega)$) and placed in series with a resistor of a known value as shown in Figure 6.11.
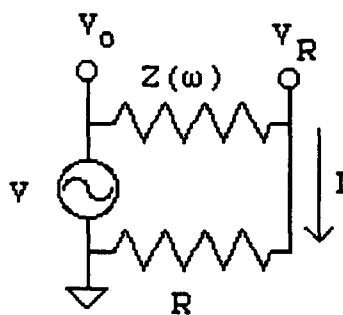
Figure 6.11 Representation of circuit used to measure the impedance of the twin-T.

Since the two resistors are in series the current in the circuit will be the same through both resistors (Horowitz and Hill, 1989, pg.32). Then the impedance in the twin-T is given by

$$Z = (V_o - V_r)\frac{R}{V_r.}$$

6.16

The resistor R nominally was a 220 k resistor whose actual measured resistance was 218.4 k. The magnitude of the twin-T's impedance for a wide frequency range are plotted in Figure 6.12. The peak maximum is approximately three orders of magnitude above the rest of the sampled range. The three order of magnitude change is approximately equal to the level shown below in Figure 6.17. This demonstrates the close matching of the actual

components since only a closely matched circuit can produce such a high Q . The resonant

frequency occurs at 1.64 kHz which is slightly different than the ideal case , but is within

10% of the desired value. The graph otherwise conforms closely to the ideal case

produced in Figure 6.17. This circuit then gives a method of producing a frequency -

dependent resistance that can be used in place of the standard feedback resistor in the

detector circuit.
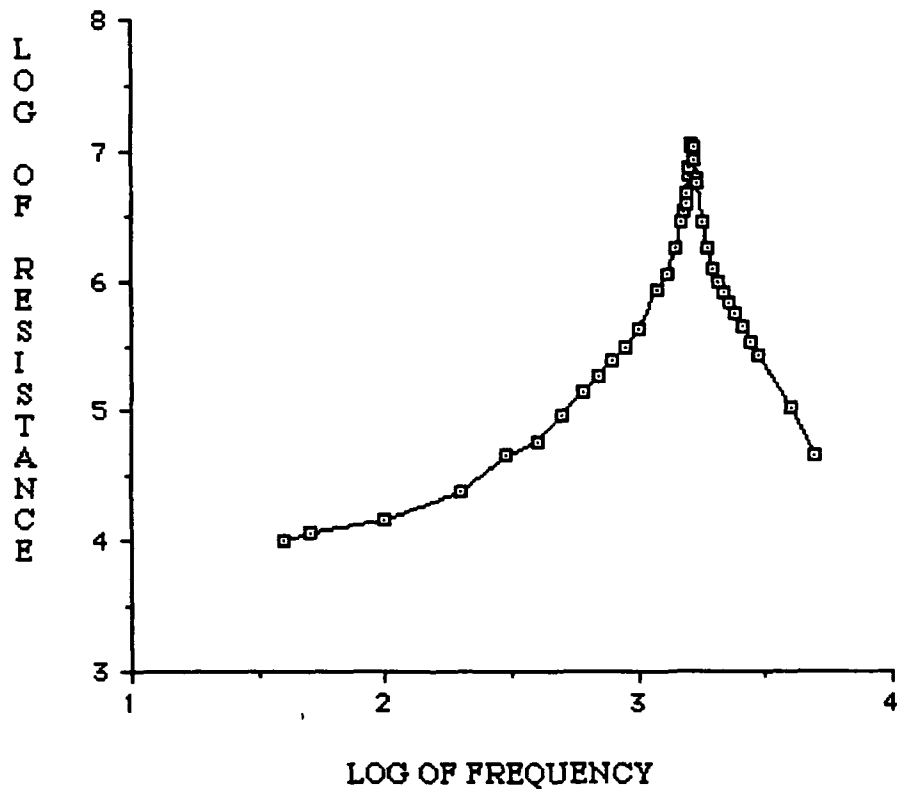
FIGURE 6.12 Resistance verses frequency response of the basic Twin-T.

F. THE MODIFIED TRANSIMPEDANCE DETECTOR CIRCUIT

Figure 6.13 shows the modified transimpedance detector system that was constructed,

using the twin - T feedback impedance described in the previous section. When it was

switched on, this circuit did not perform as expected. There were some expected

characteristics, such as a pronounced insensitivity to low frequency and DC background signals, and a greatly enhanced sensitivity at the 1.64 kHz resonant frequency.

However, the system's flaws proved to be severe. It was prone to persistent and sporadic oscillation at the resonant frequency. These oscillations were typically sinusoidal, with an amplitude of about 10 mV. The circuit's noise level at 1.64 kHz was an enormous $2\mu V/\sqrt{Hz}$, compared to 10 - 20 $nV/\sqrt{Hz}$ at other frequencies.

These observations implied that the circuit's negative feedback characteristics were being destroyed in the vicinity of the 1.64 kHz resonant frequency.
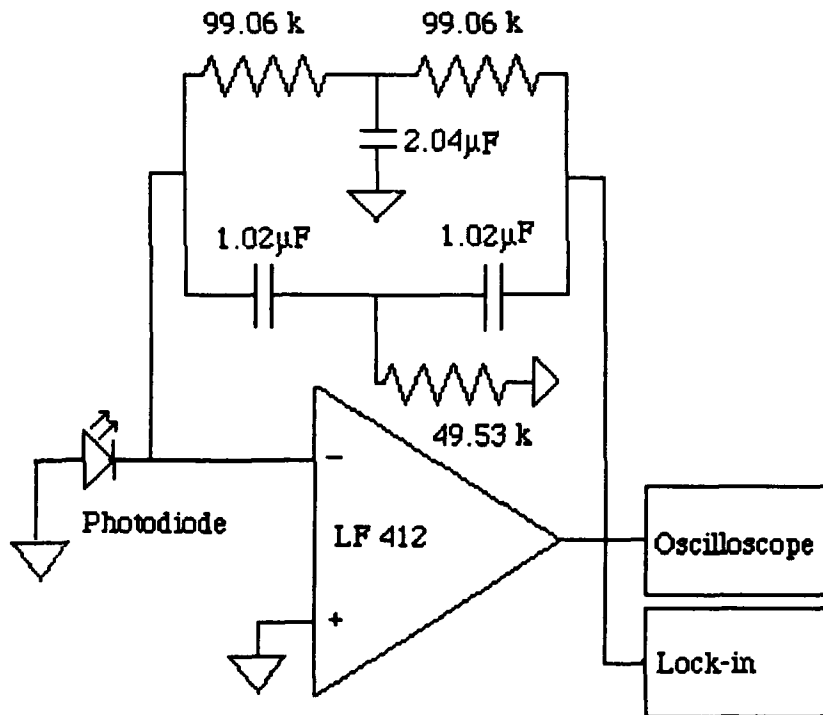
Figure 6.13 The modified detector circuit incorporating the twin-T resistor circuit.

G. CIRCUIT ANALYSIS USING MICRO-CAP II

The results given by the basic twin-T circuit were not as expected and showed that detailed numerical analysis of the circuit characteristics were necessary. The circuits were
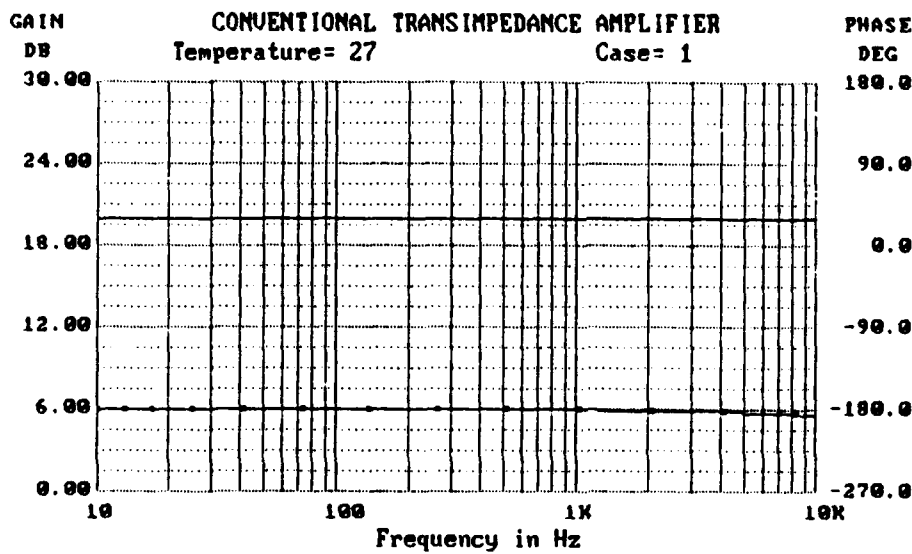
analyzed using MICRO-CAP II, an electronic circuit design software package for use on

IBM PC - compatible computer systems (Spectrum Software, 1986).

During this numerical analysis the photodiode was replaced by its Thevenin

equivalent, a resistance of 1 M in series with voltage source. This Thevenin resistance for

the photodiode was based on Section VI A above. Any capacitance of the photodiode is

not considered, since it will not affect the circuit operation over the range of frequencies of

these analyses.

The conventional transimpedance circuit in Figure 6.14 was first analyzed and the

Bode plot of the gain and phase are shown in Figure 6.15. The gain is shown as the solid

line, and the phase is shown as the solid line with boxed points. This represents what was

expected for this circuit: the gain is flat for all input frequencies, and the shift is 180° .
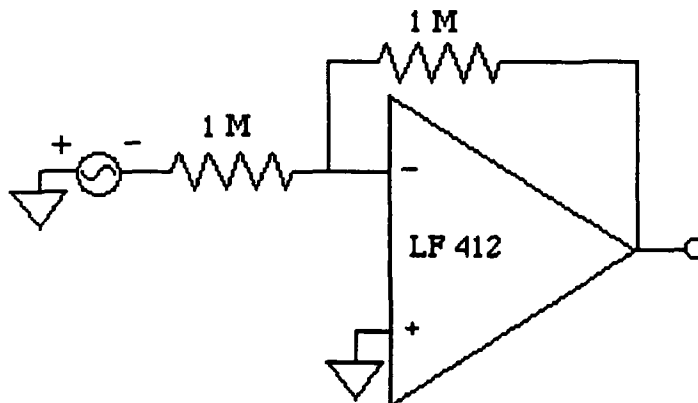
Figure 6.14   Micro-Cap II analyzed conventional transimpedance circuit.

53

```
GAIN        CONUENTIONAL TRANSIMPEDANCE AMPLIFIER      PHASE
DB          Temperature= 27                Case= 1     DEG
30.00                                                  180.0

24.00                                                  90.0

18.00                                                  0.0

12.00                                                  -90.0

6.00                                                   -180.0

0.00                                                   -270.0
    10            100            1K            10K
              Frequency in Hz
```

Frequency = 100.00000E+02 Hz   Gain   =   19.952 Db
Phase angle= -186.200   Degrees   Group delay= 173.55290E-00
Gain slope = -541.60620E-04 Db/Oct   Peak gain =   19.999Db/F= 100.00000E-01

Figure 6.15 Bode plot of phase and gain of conventional transimpedance amplifier.

The modified transimpedance circuit with the twin-T installed (Figure 6.16) was then analyzed. The circuit's gain was plotted as the solid line. The gain follows the shape that is consistent with the expected behavior of a twin-T, and the peak frequency is at approximately the predicted value. The phase, represented by the solid line with blocks, shows a problem. There is a pronounced phase shift near the resonant frequency. A phase shift in the circuit of greater than plus or minus 90° will result in net positive feedback. This will cause an oscillation that completely overwhelms any other useful circuit properties. All of these predictions agree with the observations reported in Section VI F, above. Therefore, the modified transimpedance circuit is able to provide the necessary frequency - depended characteristics for the magnitude of the feedback impedance, but the phase characteristics render the system unusable. After several additional design iterations, an alternate form of the circuit was developed and is described below.
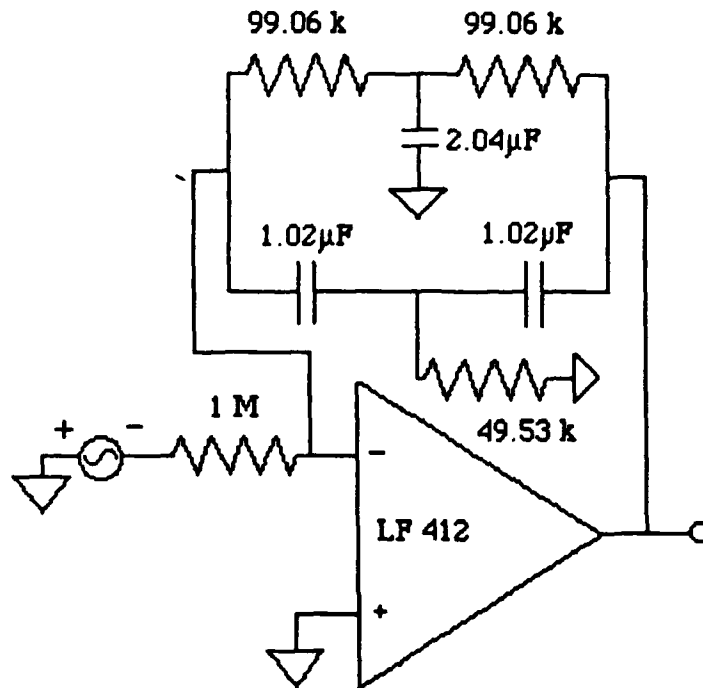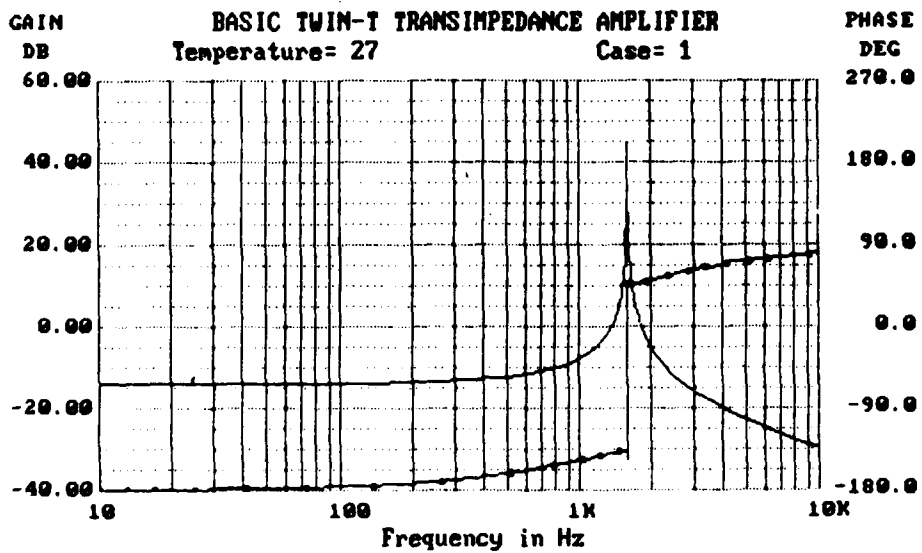
Figure 6.16 Modified transimpedance amplifier used in Micro-Cap II analysis.
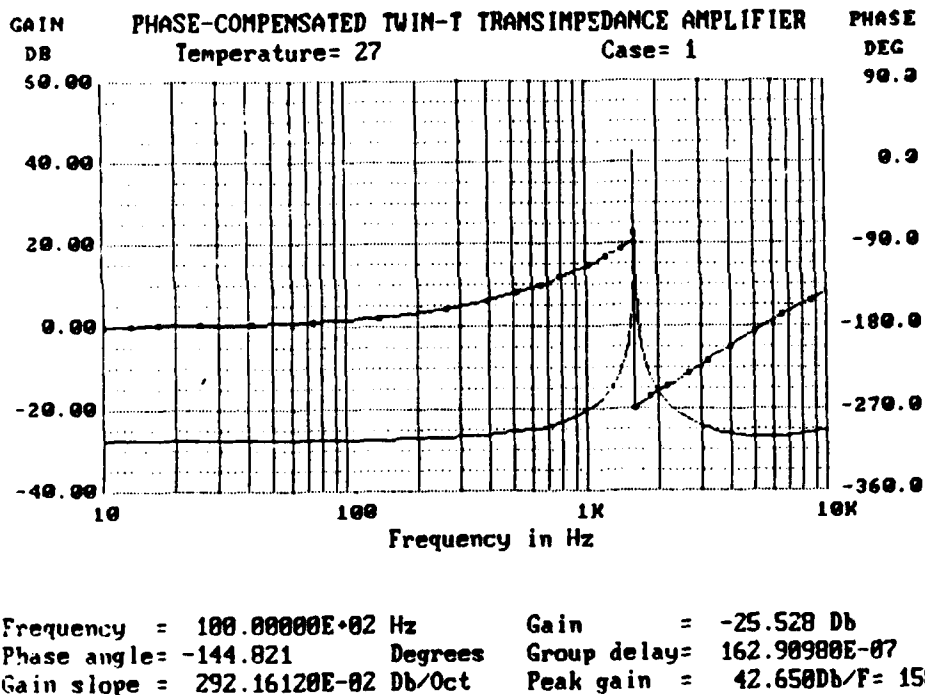

Figure = 100.00000E+02 Hz   Gain   = -29.670 Db
Phase angle=   80.387   Degrees   Group delay= 249.99200E-08
Gain slope = -651.69810E-02 Db/Oct   Peak gain =   44.845Db/F= 158.50000E+01

Figure 6.17 Bode Plot of modified twin-T circuit.

55

II. PHASE COMPENSATED TWIN-T CIRCUIT

In order to address the positive feedback problem in the basic twin-T transimpedance circuit, a phase compensation buffering network was designed. This circuit was both designed and analyzed using MICRO-CAP II and is shown below as Figure 6.19. This circuit is still has a resonant frequency just as the standard twin-T does, but its phase shifts near the resonant frequency are constrained entirely to the negative feedback regime, as shown in Figure 6.18.

Frequency = 100.00000E+02 Hz	Gain = -25.528 Db	
Phase angle= -144.821 Degrees	Group delay= 162.90900E-07	
Gain slope = 292.16120E-02 Db/Oct	Peak gain = 42.650Db/F= 158.90000E+01	

Figure 6.18   Bode plot of gain and phase verses frequency for the phase compensated transimpedance amplifier.

The phase shift created by the buffered input and outputs using two LF412 opamps ensures that the magnitudes of the phase shifts never exceed 90°. Hence, there should be no chance of positive feedback taking place in this circuit. A prototype of this circuit was constructed on a standard circuit board, with a frequency generator used as the voltage source.

56

The circuit did not perform as expected, however. It generated a sinusoidal oscillation at 10 kHz, regardless of the input signals frequency. The circuit was obviously experiencing a positive feedback condition, at a frequency far removed from the twin-T resonance. The .0068 µF capacitor, on the input buffer to the twin-T(see Figure 6.19), was varied to eliminate the positive feedback condition. A .1 µF capacitor was necessary to ensure that the circuit was not in a positive feedback condition. All available capacitors below this value still resulted in a positive feedback condition.
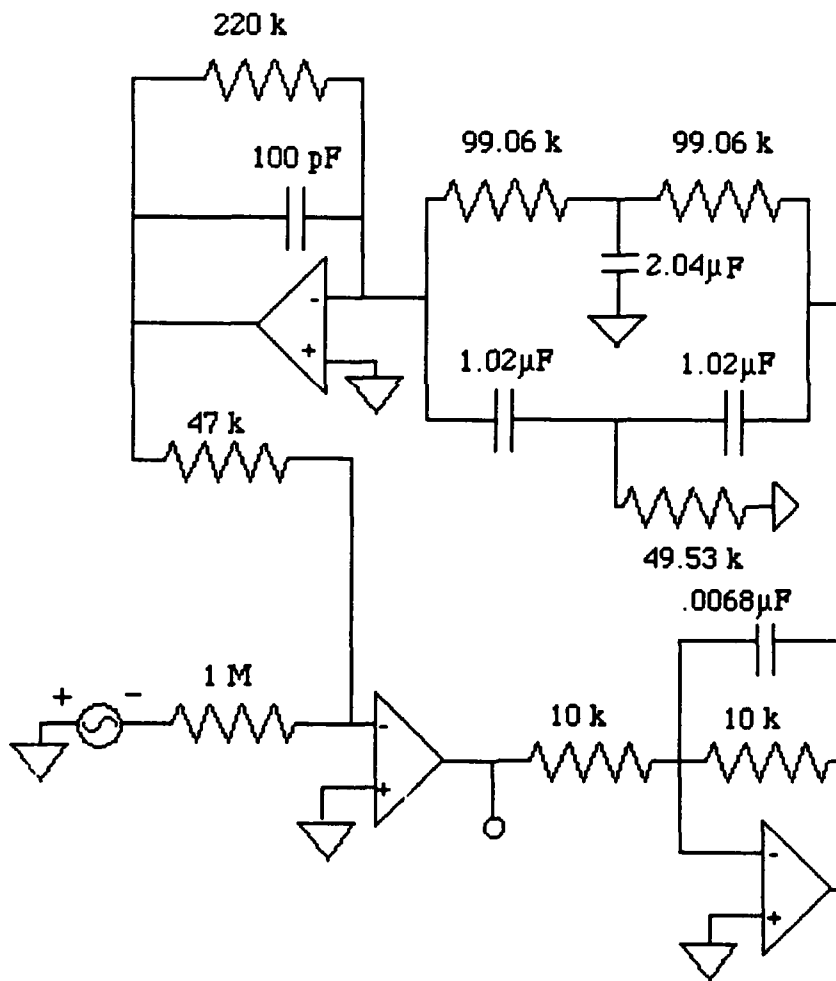
Figure 6.19 Phase compensated twin-T transimpedance amplifier used in the MICRO-CAP II circuit analyzer.
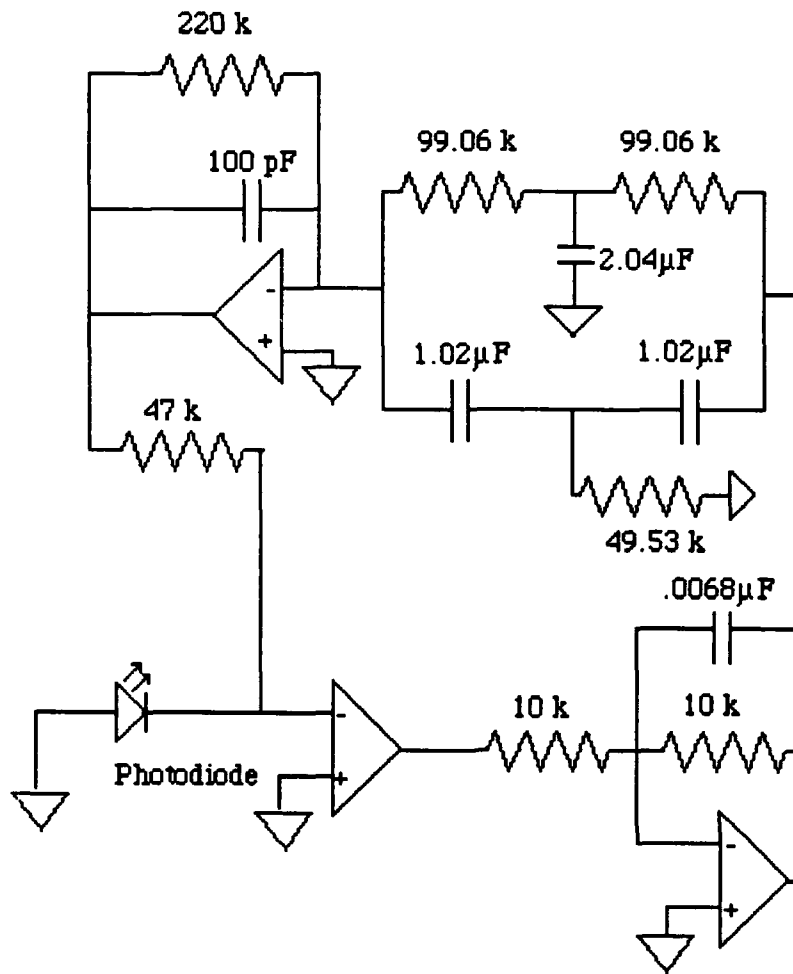
Noise measurements of the phase - compensated twin-T circuit were made with the voltage source removed and the 1 M input resistor grounded. Noise measurements of the modified circuit were made for a wide range of frequencies with both the .0068 and .1 µf capacitors . These are compiled, along with the noise measurements for the conventional transimpedance amplifier and the modified twin-T circuits, in Table 6.6.

An attempt to construct a working phase-compensated twin-T transimpedance detector system (Figure 6.20) on the breadboard resulted in the photodiode being destroyed. Time constraints and the notorious NPS procurement system prevented replacement photodiode from being purchased and tested in this circuit. It is believed that further investigation of this circuit will produce a viable background suppression circuit for use as an improved infrared detector system.

TABLE 6.6 NOISE PRODUCED BY ALL DETECTOR TYPES AT VARIOUS FREQUENCIES.

Frequency (Hz)	Conventional Detector	Twin-T Detector	Phase Compensated Detector with	
			.0068µF	.1µF
500	.3µV	14nV	.16µV	2µV
1000	.3µV	10nV	.16µV	2µV
1500	.3µV	12nV	.13µV	16µV
1675	.3µV	2µV	4.6µV	66µV
2000	.3µV	16nV	.14µV	4.5µV
3000	.3µV	17nV	.13µV	10µV

Figure 6.20 The phase compensated twin-T transimpedance amplifier

VII. CONCLUSIONS AND RECOMMENDATIONS

A. CONCLUSIONS

This thesis research attempted to develop an improved transimpedance detector that provided a frequency dependent response. Initially, we classified the noise of the conventional transimpedance detector circuit as a basis for comparison. First, the twin-T was incorporated unsuccessfully into the circuit. This method failed due to an excessive phase shift near resonance. A phase compensated transimpedance detector was designed and constructed. This circuit unexpectedly experienced positive feedback .

B. RECOMMENDATIONS

The purely electronic test of the phase-compensated twin-T transimpedance circuitry (see Section VI.H) imply that this configuration will result in a useful improvement in transimpedance detector system performance. Therefore, it is recommended that a replacement photovoltaic diode be procured, and that a thorough experimental investigation of such a system, in the presence of background signals and noise, be conducted.

An additional recommendation is made as a longer-term goal. The final form of the phase-compensated twin-T transimpedance system developed here utilizes a much larger number of basic circuit components (opamps, resistors, capacitors) than does the traditional system that it is supposed to replace. This presents three potential problems. First, the increased number of opamps and resistors provides more potential noise sources, which can degrade detector system performance. Second, a larger number of components greatly increases the system's susceptibility to failure when any single circuit element fails. Third, any working field version of the system will have to be configured into a cryogenic dewar, with the opamps on a warm surface and the other components at low temperatures. This will require great ingenuity, if long leads, stray capacitances and, microphonic pickup are

to be avoided. For these reasons, it is recommended that further design studies be initiated, in order to search for a simpler system that will meet the same performance objectives.

LIST OF REFERENCES

1. Boyd,R.W., *Radiometry and the Detection of Optical Radiation*, John Wiley and Sons, Inc.,1983.

2. Horowitz,P., and Hill,W., *The Art of Electronics*, Cambridge University Press, 2d ed, 1989.

3. Kittel,C., and Kroemer,H., *Thermal Physics*, W.H.Freeman and Co.,1980.

4. Parriott,G.R.,*Development and Testing of a Prototype Electro-Optical Phase Encoded Position Transducer*,Masters Thesis, Naval Postgraduate School, Monterey, California, December,1991.

5. Pierret,R.F., *Semiconductor Fundamentals*,2d,Addison-Wesley,1988.

6. Spectrum Software,*MICRO-CAP II Electronic Circuit Analysis Program*,1986.

7. Stanford Research Systems, *Model SR 510 Lock-In Amplifier*,1989.

8. Taylor,J.R., *An Introduction to Error Analysis*, University Science Books,1982.

9. Texas Instrument Incorporated, *Linear Circuits Data Book 1992* , v1 ,1992.

10. Towers,T., *Towers' International Resistor Selector*,3d,1989.

INITIAL DISTRIBUTION LIST

1. Defense Technical Information Center   2
   Cameron Station
   Alexandria, VA 22304-6145

2. Library, Code 52   2
   Naval Postgraduate School
   Monterey, CA 93943-5002

3. Professor K.E. Woehler, Code PH/Wh   1
   Chairman, Department of Physics
   Naval Postgraduate School
   Monterey, CA 93943-5000

4. Assoc. Professor D.S. Davis, Code PH/Dv   2
   Department of Physics
   Naval Postgraduate School
   Monterey, CA 93943-5002

5. Assoc. Professor A.A. Atchley, Code PH/Ay   1
   Department of Physics
   Naval Postgraduate School
   Monterey, CA 93943-5000

6. Department of Physics Library, Code PH   2
   Naval Postgraduate School
   Monterey, CA 93943-5000

7. LT Ferdinand J. Metzger Jr., USN   2
   909 Commodore Dr.
   Virginia Beach, VA 23430